Brain, Behavior, and Immunity xxx (2016) xxx–xxx

Contents lists available at ScienceDirect

Brain, Behavior, and Immunity

journal homepage: www.elsevier.com/locate/ybrbi

Full-length Article

Selective dentate gyrus disruption causes memory impairment at the early stage of experimental multiple sclerosis

Vincent Planche [a,b,c,*], Aude Panatier [a,b], Bassem Hiba [b,d], Eva-Gunnel Ducourneau [a,b], Gerard Raffard [b,e], Nadège Dubourdieu [a,b], Marlène Maitre [a,b], Thierry Lesté-Lasserre [a,b], Bruno Brochet [a,b,f], Vincent Dousset [a,b,f], Aline Desmedt [a,b], Stéphane H. Oliet [a,b], Thomas Tourdias [a,b,f]

[a] INSERM, U1215, Neurocentre Magendie, F-33000 Bordeaux, France
[b] Univ. Bordeaux, F-33000 Bordeaux, France
[c] CHU de Clermont-Ferrand, F-63000 Clermont-Ferrand, France
[d] CNRS UMR 5287, Institut de Neurosciences Cognitives et Intégratives d'Aquitaine, F-33000 Bordeaux, France
[e] CNRS UMR 5536, Centre de Résonance Magnétique des Systèmes Biologiques, F-33000 Bordeaux, France
[f] CHU de Bordeaux, F-33000 Bordeaux, France

ARTICLE INFO

Article history:
Received 11 July 2016
Received in revised form 7 November 2016
Accepted 12 November 2016
Available online xxxx

Keywords:
Multiple sclerosis
Experimental autoimmune encephalomyelitis
Hippocampus
Dentate gyrus
Memory impairment
Synaptic plasticity
Microglia
Diffusion tensor imaging

ABSTRACT

Memory impairment is an early and disabling manifestation of multiple sclerosis whose anatomical and biological substrates are still poorly understood. We thus investigated whether memory impairment encountered at the early stage of the disease could be explained by a differential vulnerability of particular hippocampal subfields. By using experimental autoimmune encephalomyelitis (EAE), a mouse model of multiple sclerosis, we identified that early memory impairment was associated with selective alteration of the dentate gyrus as pinpointed *in vivo* with diffusion-tensor-imaging (DTI). Neuromorphometric analyses and electrophysiological recordings confirmed dendritic degeneration, alteration in glutamatergic synaptic transmission and impaired long-term synaptic potentiation selectively in the dentate gyrus, but not in CA1, together with a more severe pattern of microglial activation in this subfield. Systemic injections of the microglial inhibitor minocycline prevented DTI, morphological, electrophysiological and behavioral impairments in EAE-mice. Furthermore, daily infusions of minocycline specifically within the dentate gyrus were sufficient to prevent memory impairment in EAE-mice while infusions of minocycline within CA1 were inefficient. We conclude that early memory impairment in EAE is due to a selective disruption of the dentate gyrus associated with microglia activation. These results open new pathophysiological, imaging, and therapeutic perspectives for memory impairment in multiple sclerosis.

1. Introduction

Multiple sclerosis is the most frequent inflammatory disorder of the central nervous system (Compston and Coles, 2008). Among symptoms, episodic memory impairment is frequent (Planche et al., 2016), greatly impacts quality of life (Ruet et al., 2013) and occurs early during the course of the disease (Feuillet et al., 2007). Evidence from clinical studies links episodic memory impairment with hippocampal alteration. Nevertheless, these human data are either post-mortem histological studies inherently biased toward the chronic stage of the disease (Papadopoulos et al., 2009; Dutta et al., 2011), or *in vivo* studies based on measurement of hippocampal atrophy on magnetic resonance imaging (MRI), which reflects again a late process and don't inform on the underlying cellular modifications (Sicotte et al., 2008; Koenig et al., 2014). Therefore, there is a need for a better understanding of the substrate of early memory deficit associated with multiple sclerosis.

The cellular mechanisms that could be potentially disrupted in the hippocampus during the early stage of multiple sclerosis are mainly those involved in long-term synaptic plasticity within the trisynaptic loop, which is one of the major substrates for learning and memory (Citri and Malenka, 2008). These mechanisms can only be explored by using experimental autoimmune encephalomyelitis (EAE), the most widely accepted animal model of multiple sclerosis ('t Hart et al., 2011). Early synaptic dysfunctions have

* Corresponding author at: Neurocentre Magendie, Inserm U1215, 146 Rue Léo Saignat, 33000 Bordeaux, France.
E-mail address: planche.vincent@gmail.com (V. Planche).

http://dx.doi.org/10.1016/j.bbi.2016.11.010
0889-1591/

been reported in EAE and associated with pro-inflammatory cytokines released by macrophages, microglia or astrocytes (Centonze et al., 2009; Nisticò et al., 2013; Di Filippo et al., 2016; Habbas et al., 2015), leading to the concept of "inflammatory synapthopathy" (Mandolesi et al., 2015). However, it is currently unknown whether some particular synaptic pathways could be differentially targeted by activated glial cells during the course of multiple sclerosis or EAE.

Indeed, the hippocampus is composed of different interconnected regions and layers (the Cornu Ammonis subfields, the dentate gyrus and the subiculum) which are very different in their morphological, molecular, electrophysiological and functional profiles. This implies that it is not enough to consider the hippocampus as a unitary and homogeneous entity. By analogy with other diseases such as Alzheimer or post-traumatic stress disorder that differentially target distinct subregions of the hippocampus circuit, we can envision that groups of hippocampal neurons are afflicted at the early stage of multiple sclerosis while neighboring ones are not (Small et al., 2004; Small, 2014). Human MRI data also suggest that some hippocampal regions could be more affected than others in multiple sclerosis because some authors have reported hippocampal volume loss localized to specific subfields (Sicotte et al., 2008; Gold et al., 2010; Longoni et al., 2015; Rocca et al., 2015). However, these studies provide controversial results which may come from measure of atrophy performed at different stages and with different methodology. Whether hippocampal regions/subfields could be differentially vulnerable to early pathophysiological mechanisms in multiple sclerosis (prior to atrophy) is therefore currently unclear and can only be addressed with the EAE model.

Consequently, in this study, we looked for the substrate of early memory impairment in multiple sclerosis by combining multi scale complementary approaches in the different hippocampal subfields of EAE-mice. Similarly to the human disease, we demonstrated that EAE-mice showed hippocampal-dependent memory impairment prior to hippocampal atrophy. Then, we used diffusion tensor imaging (DTI) as an *in vivo* "screening procedure" to pinpoint potential regional vulnerability and focus the other experiments. We identified the locus of early hippocampal disruption in the dentate gyrus with concordant DTI, morphological and electrophysiological experiments. This selective vulnerability was associated with early microglial activation and was prevented with systemic injections or local intra-dentate gyrus infusions of the microglial inhibitor minocycline. Hence, we identified the anatomical source of memory impairment in early multiple sclerosis which could be exploited to clarify pathogenesis and which could be translated to patients as it can be captured with *in vivo* imaging.

2. Materials and methods

2.1. Animals and experimental autoimmune encephalomyelitis (EAE)

Experiments were performed on 7–9-week-old females C57BL6/J (Janvier Labs). EAE was induced with a subcutaneous injection of 150 µg of Myelin Oligodendrocyte Glycoprotein peptide 35–55 (MOG35-55, Anaspec) emulsified in 150 µL of Complete Freund's Adjuvant (CFA, Difco) containing 6 mg/mL of desiccated *Mycobacterium tuberculosis* (H37Ra, Difco). Animals received intraperitoneal (IP) injections of Pertussis Toxin (Sigma) on the day of immunization and 2 days later (250 ng/injection). Control mice were injected with 150 µL of CFA emulsified in phosphate-buffered saline (PBS). All animals were weighted daily and scored for clinical symptoms using the standard grading scale: 0, unaffected; 1: flaccid tail; 2: hind limb weakness and/or ataxia; 3: hind limb paralysis; 4: paralysis of all four limbs and 5: moribund.

All experiments reported in this article were performed early in the course of the disease at 20 days post-injection (d.p.i), except electrophysiological experiments which were performed between 18 and 22 d.p.i. All animal care and experiments were conducted in accordance with the European directive (2010/63/EU) and after approval of the local ethical committee (approval number 02046.01).

2.2. Contextual fear conditioning

Memory functions were assessed with a particular contextual fear conditioning procedure (Fig. 1B) that does not require important motor skills unlike other tests, such as the Morris water maze. Acquisition of fear conditioning took place in a Plexiglas box (30 × 24 × 22 cm, Imetronic) in a brightness of 60 lx, given access to different visual-spatial cues in the experimental room. The floor of the chamber consisted of stainless-steel rods connected to a shock generator. The box was cleaned with 70% ethanol. The training procedure consisted on a pseudo-random distribution of tones and shocks as followed (tone-shock unpairing procedure): 100 s after being placed into the chamber, animals received a footshock (0.4 mA squared signal, 1 s), then, after 20 s, a tone (65 dB, 1 kHz, 15 s) was presented twice (30 s delay); finally, after 30 s, mice received a second shock and returned to the home cage 20 s after. One day after the acquisition, mice were re-exposed to the tone alone during 2 min in a safe and familiar chamber where they had been pre-exposed the day before conditioning (opaque PVC chamber with opaque floor, brightness of 15 lx, cleaned with 4% acetic acid). One hour later, animals were re-exposed to the conditioning context alone, without the tone. Animals were recorded on videotape for off-line manual scoring of freezing behavior. We previously repeatedly showed that such conditioning procedure normally leads to the identification of the conditioning context as the correct predictor of the threat (*i.e.* footshock) as animals display conditioned fear when re-exposed to the context but not to the discrete tone (Calandreau et al., 2006; Desmedt et al., 1999; Kaouane et al., 2012).

Conditioned fear to the context was assessed by measuring the percentage of total time spent freezing during the first 2 min period of context re-exposure. In order to assess conditioned fear to the tone, a freezing ratio was calculated as follow: [% freezing during the tone presentation − (% pre-tone period freezing + % post-tone period freezing)/2]/[% freezing during the tone presentation + (% pre-tone period freezing + % post-tone period freezing)/2]. Two different observers performed the measurements independently and blinded of experimental groups (EAE, n = 12 and CFA, n = 12).

Slowing of information processing speed is frequent in multiple sclerosis (Chiaravalloti and DeLuca, 2008) and can confound memory tests. Thus, we reasoned that EAE-mice could need more time than CFA-mice to process and memorize a new context independently of hippocampal dysfunction. To disentangle these phenomena, we designed a new experimental procedure where the conditioning period was longer: 130 s into the chamber, first shock, 40 s delay, first tone, 50 s delay; second tone, 50 s delay, second shock, 20 s and back to the home cage. Tone, shock, context parameters and testing conditions were the same as described above (EAE, n = 12 and CFA, n = 12).

2.3. Magnetic resonance imaging: acquisition and analyses

The afternoon following contextual fear conditioning, the same animals underwent MRI exploration. Imaging was performed on a 4.7T scanner (Biospec 47/20, Brucker) equipped with a high-performance gradient system (capable of 660 mT/m maximum strength and 110 µs rise time). A 86 mm-diameter volume coil

Please cite this article in press as: Planche, V., et al. Selective dentate gyrus disruption causes memory impairment at the early stage of experimental multiple sclerosis. Brain Behav. Immun. (2016), http://dx.doi.org/10.1016/j.bbi.2016.11.010

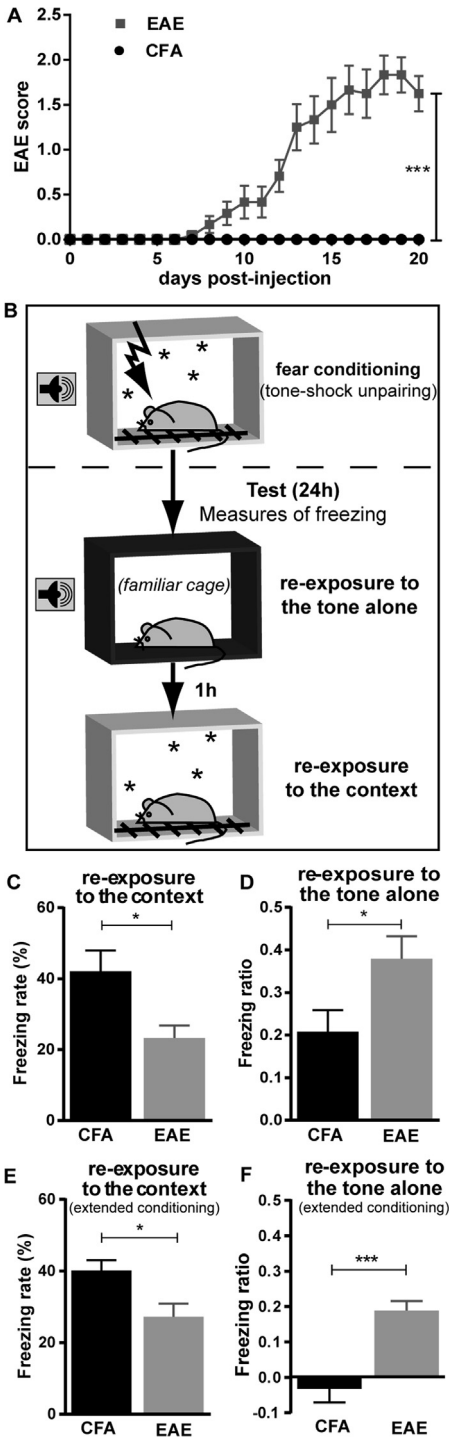

Fig. 1. Clinical and memory-related behavioral data of mice with experimental autoimmune encephalomyelitis (EAE) and control mice (CFA). (A) Motor signs began 7 days post-injection (d.p.i) and were moderately severe at 20 d.p.i. when mice were tested for memory performances ($^{***}p < 0.001$, $F = 41.61$, two-way ANOVA, $n = 12$ per group). (B) Schematic representation of the contextual fear conditioning paradigm: because the discrete tone and the footshock are pseudo-randomly distributed (tone-footshock unpairing), the background context is the only predictive factor of the footshock occurrence. Acquisition of an adaptive conditioned fear to the context is attested 24 h later when mice are re-exposed to the discrete tone alone in a familiar context, then to the conditioning context alone. (C) EAE-mice displayed less conditioned freezing to the predictive conditioning context than CFA-mice. (D) However, EAE-mice exhibited a paradoxical and maladaptive freezing behavior to the tone when re-exposed to it in a familiar and safe box. (E and F) The same differences between groups were observed even if time exposure to the context was extended by 40%. ($^{*}p < 0.05$ and $^{***}p < 0.001$, *t*-test, $n = 12$ per group.)

was used for radio frequency pulse transmission and a four-elements phased array surface coil for signal detection. Mice anesthetized with isoflurane in air (1–2% concentration to obtain a respiratory rate between 25/s and 35/s) were immobilized in a head holder with ear bars and their body temperature was kept at 37 °C.

We first collected standard T2-weighted images to assess hippocampal volumetry. This was acquired using a fat-suppressed turbo spin echo axial sequence (Turbo-RARE, TR = 4843 ms, effective TE = 66 ms, matrix = 196 × 196 pixels, FOV = 20 × 16 mm^2, spatial resolution = 102 × 82 × 300 μm, 15 averages, 25 axial slices, scan time = 14 min 32 s).

To analyze microstructural changes in the three main hippocampal layers (*i.e.* the stratum radiatum, the stratum lacunosum-moleculare and the molecular layer of the dentate gyrus), we designed and optimized a new DTI pulse sequence based on a 3D-sampling of Fourier-space. Each of these hippocampal layers is about 200 μm thick in the coronal plane, oriented perpendicular to the longitudinal axis of the dorsal hippocampus. We postulated that the in-plane resolution of the obtained diffusion-weighted images should be less than 100 μm, to get at least 2 voxels per layer in the dorso-ventral axis. Because of little through-plane anatomical variation of the hippocampus in its dorsal part, we favored in-plane resolution with thicker slices to recover enough signal (anisotropic voxel). Furthermore, we favored a high b-value in a high number of directions, to be more sensitive to restricted diffusion in a complex and heterogeneous structure such as the hippocampus (Shepherd et al., 2006). We obtained the best tradeoff between signal-to-noise ratio, scan time, spatial resolution and b-value with a multi-shot echo-planar-imaging (EPI) pulse sequence as follow: TR = 2000 ms, TE = 38 ms, matrix = 196 × 148, FOV = 16 × 12 mm^2, 2 segments, spatial resolution = 82 × 81 × 203 μm, 32 coronal slices including the whole hippocampus in the rostro-caudal axis. Two images without diffusion weighting were acquired and 30 images with diffusion weighting ($\Delta = 10$ ms, $\delta = 3$ ms, b-value 2000 s/mm^2) were collected in 30 different diffusion directions. All exams began with a higher order shim procedure to optimize first and second order shims based on a 3D field map acquired over the whole brain. The total acquisition time for *in vivo* DTI was 51 min 12 s.

Images were post-processed off-line for volumetric analyses and extraction of diffusion metrics within each hippocampal layer. T2-weighted images were analyzed using the 3D-Slicer software (slicer.org). Hippocampal boundaries were manually traced on contiguous axial slices by an investigator blinded of the experimental conditions. Diffusion-weighed data were processed and analyzed using FMRIB Software Library (FSL, fmrib.ox.ac.uk). Eddy current distortions were firstly corrected and then, the diffusion tensor was calculated using mono-exponential diffusion tensor model. Color-coded fractional anisotropy (FA) maps were used to manually outline regions of interest (ROIs) in the stratum radiatum of CA1, stratum lacunosum-moleculare and molecular layer of the dentate gyrus, on 3 consecutive slices, within the dorsal part of the hippocampus (known to be the part of the hippocampus linked to memory processes (Kheirbek et al., 2013)) (Fig. 2A and B). CA3 hippocampal subfield was not properly analyzed because of its rotation in the coronal plane that does not allow its clear individualization in color-coded FA maps. Right and left hippocampi were averaged because no difference was observed between the two sides. The mean FA, the mean eigenvalues ($\lambda 1$, $\lambda 2$, $\lambda 3$) and the mean diffusivity within the ROIs were obtained using FSL and then, axial ($\lambda 1$) and radial diffusivity ($(\lambda 2 + \lambda 3)/2$) were calculated. The analysis was performed blinded of the animal groups (EAE, CFA, treatment) and all the measures were repeated twice, one month apart, with very good reproducibility (intra-class correlation coefficient was 0.80 for FA and 0.97 for axial

Please cite this article in press as: Planche, V., et al. Selective dentate gyrus disruption causes memory impairment at the early stage of experimental multiple sclerosis. Brain Behav. Immun. (2016), http://dx.doi.org/10.1016/j.bbi.2016.11.010

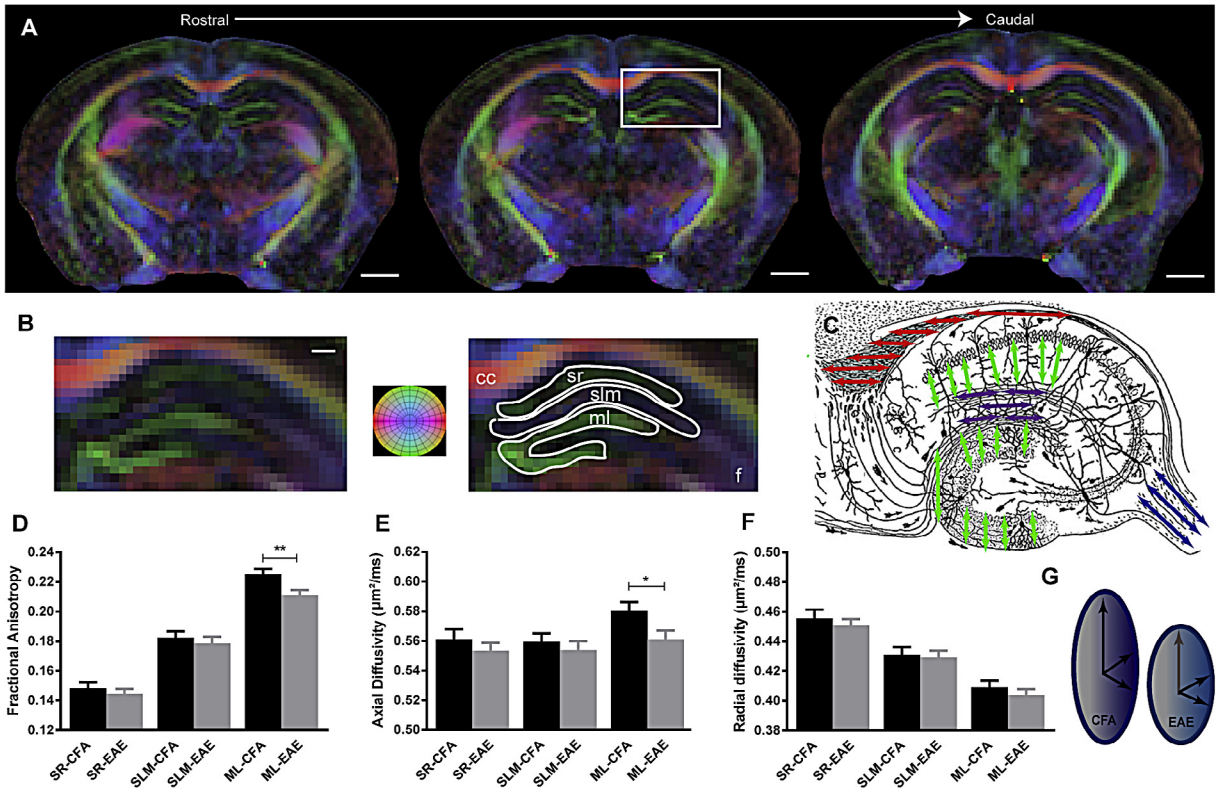

Fig. 2. Diffusion-tensor imaging (DTI) of hippocampal layers revealed microstructural damages specific to the molecular layer of the dentate gyrus. (A) Color-coded fractional anisotropy (FA) maps were used to draw 3 regions of interest (ROIs) within the hippocampus. The dorsal part of the right and left hippocampi were analyzed in three adjacent slices for each animal, along the rostro-caudal axis. (B) Magnification of the white box in (A) with the 3 ROIs overlaid in white. Directions for color-coding: blue, rostro-caudal; red, left-right; and green, dorsal–ventral. (C) Drawing adapted from Ramon and Cajal (1911) representing the orientation of the fibers within the different layers of the hippocampus and corroborating the color-coded FA map. (D–F) Quantification of FA, axial diffusivity (AD) and radial diffusivity in the three different ROIs for both EAE and CFA-mice. (G) Schematic representation of the tensor in the molecular layer of CFA and EAE-mice: diffusion directionality is decreased in EAE (lower FA) because of a loss of directivity in the main axis (lower AD). SR: stratum radiatum of CA1, SLM: stratum lacunosum-moleculare, ML: molecular layer of the dentate gyrus, cc: corpus callosum and f: fimbria. ($^{*}p < 0.05$, $^{**}p < 0.01$, *t*-test, n = 12 animals per group). Scale bar: 1 mm (A) and 200 μm (B). (For interpretation of the references to color in this figure legend, the reader is referred to the web version of this article.)

diffusivity (AD)). The two measured values were averaged to perform further statistical analyses.

2.4. Immunohistochemistry

To allow MRI-histological correlations, animals were sacrificed immediately following MRI. Mice were deeply anesthetized with pentobarbital and perfused transcardially with a phosphate-buffered solution containing 2% paraformaldehyde and 0.2% picric acid, for 20 min. The brain and the spinal cord were then removed and transferred into a Tris-buffered saline (TBS) containing 30% sucrose and 0.05% sodium azide and left at 4 °C until use. A 0.8 mm block containing the dorsal hippocampus (*i.e.*; from approximately bregma −1.34 to bregma −2.14 in the Paxino's atlas) was cut using 30 μm thick coronal sections on a freezing microtome. For direct comparison, both MRI and histological sections were perpendicular to the flat skull position.

For immunofluorescence, free-floating sections were rinsed in TBS and then incubated in a solution of 0.25% Triton X-100 and 1% normal donkey serum with the primary antiserum overnight. After incubation, tissue sections were washed in TBS and incubated with the appropriate secondary antibody solution (0.25% Triton X100) for 2 h. The following primary antibodies were used: rabbit anti-MBP for myelin (Myelin Basic Protein, ab 40390, Abcam, 1:1000), mouse anti-SMI-32 for dendrites (Neurofilament H non-phosphorylated, SMI-32R, Sternberger, Covance, 1:1500), rabbit anti-GFAP for astrocytes (Glial Fibrillary Acid Protein, Z0334, Dako, 1:1000), rabbit anti-Iba1 for microglia (Ionized calcium-binding Adaptor molecule 1, 019-19741, Wako, 1:2000), rabbit anti-CD3 for T lymphocytes (ab 5690, Abcam, 1:200), rat anti-ED1 for macrophages (anti-CD-68, MCA 1957, AbD Serotec, 1:200), goat anti-DCX for immature neurons (Doublecortin, sc-8066, Santa Cruz, 1:1000) and rabbit anti-active Caspase 3 for apoptosis (ab 13847, Abcam, 1:1000). The following secondary antibodies were used (donkey IgGs): anti-mouse Alexa Fluor-568 (ab 175472, Abcam, 1:1000), anti-rabbit Alexa Fluor 488 (711-545-152, Jackson Laboratories, 1:1000), anti-goat Cyanine 3 (705-165-003, Jackson Laboratories, 1:1000), anti-rat DyLight 488 (712-485-150, Jackson Laboratories, 1:500) and anti-rat Rhodamine Red-X (712-295-150, Jackson Laboratories, 1:500).

2.5. Histological processing and neurolucida reconstruction

Shortly after being processed, sections were imaged for quantitative analyses with a video-spinning-disk laser confocal microscope (Leica DMI 6000) equipped with a 20× objective and with a camera Coolsnap HQ2 (Photometrics). These systems were driven by Metamorph software (Molecular Devices) and the "scan slide" technique was used in order to visualize and reconstruct the whole hippocampus (mosaic images) for layer analyses. Individual optical sections of 1 μm were acquired and analyzed. Identical laser intensity and exposure settings were applied to all images taken for each experimental set. For all immunostaining experiments, at least 2 slices containing the dorsal hippocampus were randomly

Please cite this article in press as: Planche, V., et al. Selective dentate gyrus disruption causes memory impairment at the early stage of experimental multiple sclerosis. Brain Behav. Immun. (2016), http://dx.doi.org/10.1016/j.bbi.2016.11.010

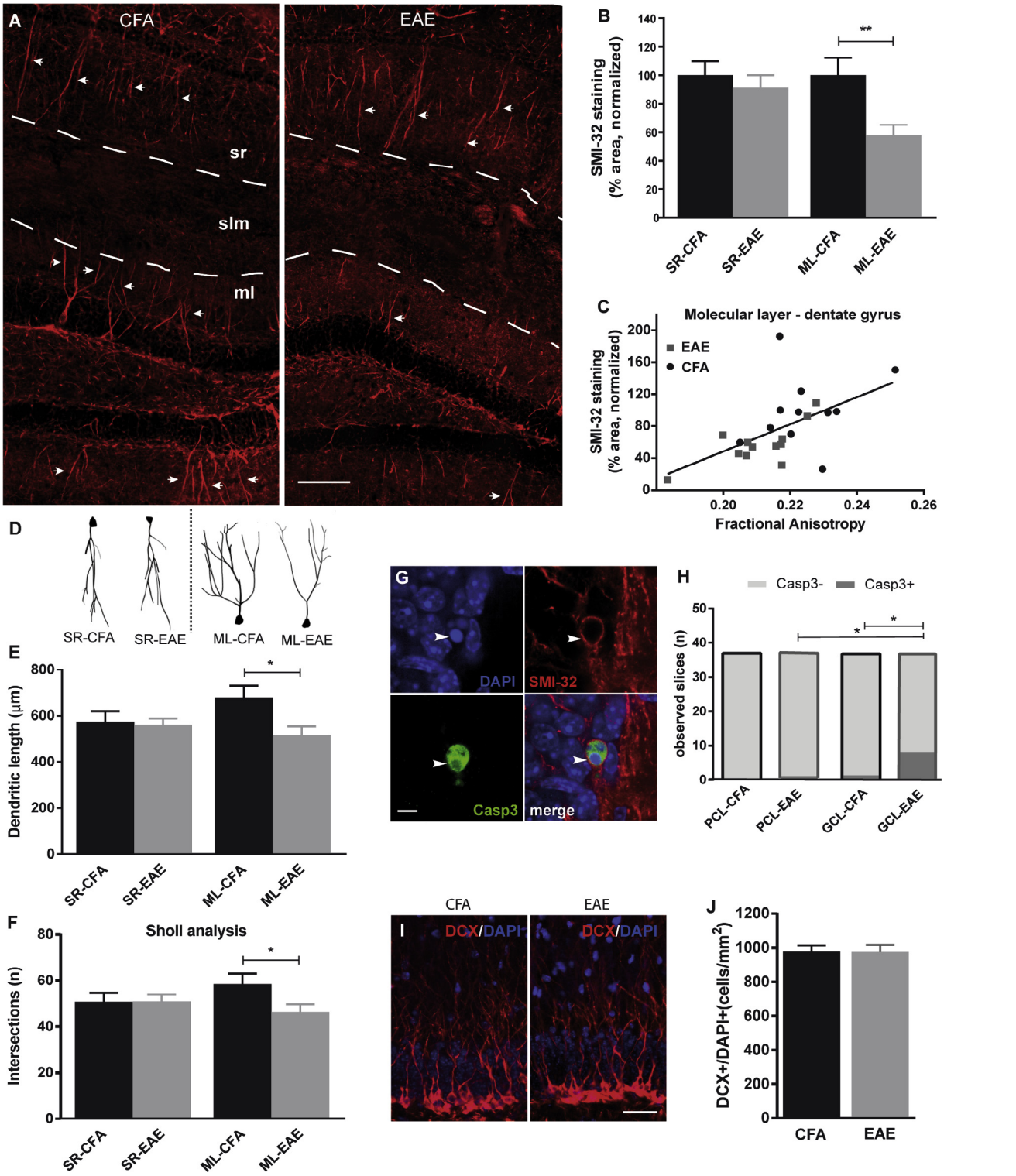

Fig. 3. Selective dendritic loss and neuronal death in the dentate gyrus of EAE-mice. (A) Immunofluorescence staining for the dendritic marker SMI-32; white arrowheads show dendrites in the different layers. (B) Quantification of SMI-32 staining area in the stratum radiatum (SR) and the molecular layer (ML) in EAE and CFA-mice ($^{**}p < 0.01$, *t*-test, n = 12 per group). The stratum lacunosum-moleculare (SLM) contains thin axons of the perforant path, which are not stained by SMI-32. (C) Correlation between SMI-32 staining and fractional anisotropy in the molecular layer of the dentate gyrus (r = 0.56, p = 0.0051, Pearson). (D–F) Neurolucida neuron tracing analyses with (E) quantification of the total dendritic length per neuron and (F) the number of intersections between dendrites and the surface of spheres with a radius increment of 10 µm ($^{*}p < 0.05$, *t*-test, n = 24 neurons per condition, from 12 animals) (see also Fig. A.3). Representative tracing of apical dendrites are shown in (D): dendrites from pyramidal cells of the pyramidal layer of CA1 and dendrites from the granular cells of the dentate gyrus. (G) Illustration of an apoptotic neuron in the granular layer of the dentate gyrus with nuclear (DAPI) and cytoplasmic (SMI-32) condensations (arrowheads), together with an intense activated-caspase 3 staining. (H) Contingency of Caspase 3+ neurons in the granular cell layer (GCL) of the dentate gyrus and the pyramidal cell layer (PCL) of CA1 was reported to the number of observed slices ($^{*}p < 0.05$, Fischer's exact test, n = 36 per condition). (I) Immunofluorescence staining for doublecortin (DCX), a marker of immature neurons. (J) DCX/DAPI cell counting did not show any difference between EAE and CFA-mice (n = 12 per group).

Please cite this article in press as: Planche, V., et al. Selective dentate gyrus disruption causes memory impairment at the early stage of experimental multiple sclerosis. Brain Behav. Immun. (2016), http://dx.doi.org/10.1016/j.bbi.2016.11.010

selected and quantitative results were averaged. Images were analyzed using ImageJ software (imagej.nih.gov). Similar ROIs as the ones used in MRI studies were manually drawn on the mosaic. Within the ROIs, the number of microglial cells (Iba1+/DAPI+), astrocytes (GFAP+/DAPI+) were counted manually and normalized by the size of the ROI. GFAP, Iba1, MBP and SMI-32 staining area were quantified automatically as percent area of immunoreactivity (after subtracting background and thresholding identically all the images for conversion to binary masks). The dendritic marker SMI-32 (non-phosphorylated neurofilament H) is widely used in multiple sclerosis and EAE pathological studies, including hippocampal exploration (Dutta et al., 2011) and provides a sparse labeling of mature dendrites and perikarya in both pyramidal and granular neurons (Mikuni et al., 1998), facilitating the analysis. DCX+/DAPI+ neuroblasts and immature neurons (respectively DCX + perikarya with short processes parallel to the longest axis of the granular cell layer or with a perpendicular process reaching the molecular layer) were counted manually within the subgranular and granular layer of the dentate gyrus and normalized by the size of the granular layer.

To provide further quantification of the dendritic arbor, the morphometric analyses of SMI-32+ neurons were performed with a 40× objective using a manual neuron tracing system (NeuroLucida, MBF Bioscience). Two neurons per animal (n = 24 per condition) were analyzed within the molecular layer of the dentate gyrus and the stratum radiatum. Neurons were selected based on the standard following criteria: (*i*) the cell body should be contained in the slice, (*ii*) the dendrites should be vertically oriented within the molecular layer or the stratum radiatum, (*iii*) the overlap with the dendrites of the adjacent cells should be minimal, to avoid ambiguous tracing of the dendritic tree. The complexity of the dendritic trees was analyzed using the concentric analysis of Sholl (Neuroexplorer). For each neuron, the total dendritic length and the total number of intersections between dendrites and the surface of concentric spheres with a radius increment of 10 µm were analyzed.

To detect apoptotic neurons, observation and quantification of Caspase-3+/SMI-32+ cell bodies were performed on epifluorescence microscope (Zeiss Axiophot 1) with a 40x objective. Because the occurrence of Caspase-3 expression was low, two to four hippocampal sections per animal were screened (n = 36 per condition), in different focal planes, in the granular layer of the dentate gyrus and in the pyramidal layer of CA1. Only the occurrence of typical staining (with nuclear and cytoplasmic condensations) was taken into account for quantitative analyses.

To obtain illustrative images (SMI-32/Iba-1 and Caspase-3/SMI-32 co-stainings), a 63x-oil objective was used and z-stack acquisitions were performed on the station previously described.

2.6. Laser capture microdissection (LCM) and quantitative real-time PCR (qPCR) analyses

For RNA analyses other EAE and CFA mice were followed and their brains were quickly extracted, flash-frozen in a vial of isopentane that was immersed in dry ice and subsequently stored at −80 °C until sectioning. Brains were cut using 50 µm thick coronal sections on a freezing microtome (CM3050 S Leica) at −22 °C to prevent RNA degradation. Tissue sections were mounted on PEN-membrane 1 mm glass slides (P.A.L.M. Microlaser Technologies AG, Bernried, Germany) that had been pretreated to inactivate RNase. Frozen sections were fixed in a series of precooled ethanol baths (40 s in 95%, 75% and 30 s in 50%) and stained with cresyl violet 1% for 20 s. Subsequently, sections were dehydrated in a series of precooled ethanol baths (30 s in 50%, 75% and 40 s in 95% and in anhydrous 100% twice). Immediately after dehydration LCM was performed with a P.A.L.M MicroBeam microdissection system version 4.0-1206 equipped with a P.A.L.M. RoboSoftware (P.A.L.M. Microlaser Technologies AG, Bernried, Germany). Laser power and duration were adjusted to optimize capture efficiency. Microdissection was performed at 5× magnification. The molecular layer of the dentate gyrus and the stratum radiatum of the CA1 were selectively captured (see Supplementary method A.1 for example) in adhesive caps (P.AL.M Microlaser Technologies AG, Bernried, Germany). Following LCM, 150 µl of extraction buffer provided in a ReliaPrep™ RNA Cell Miniprep System (Promega) were added to the caps and stored at −80 °C until RNA isolation. Total RNA was extracted from microdissected tissues by using the ReliaPrep™ RNA Cell Miniprep System (Promega, Madison, USA) according to the manufacturer's protocol and eluted with 14 µl of RNAse-free water. The concentration of RNA was determined with Nanodrop 1000. RNA qualities were performed using Agilent RNA 6000 Pico Kit on 2100 Bioanalyzer (Agilent Technologies, Santa Clara, CA).

RNA was processed and analyzed according to an adaptation of published methods (Bustin et al., 2009). Briefly, cDNA was synthesized from 75 ng of total RNA for each structure by using qSript™ cDNA SuperMix (Quanta Biosciences). qPCR was performed with a LightCycler® 480 Real-Time PCR System (Roche, Meylan, France). qPCR reactions were done in duplicate for each sample by using LightCycler 480 SYBR Green I Master (Roche) in a final volume of 10 µl. The qPCR data were exported and analyzed in an informatics tool (Gene Expression Analysis Software Environment) developed at our institute. The Genorm method was used to determine the reference gene (Bustin et al., 2009). Relative expression analysis was normalized against two reference genes. In particular, succinate dehydrogenase complex subunit (Sdha) and non-POU-domain-containing, octamer binding protein (Nono) were used as reference genes. To estimate the PCR amplification efficiency, standard curves were determined, and all the primers chosen were 100% efficient. The relative level of expression was calculated with the comparative ($2^{-\Delta\Delta CT}$) method (n = 4–10 animals per analyses). Primer sequences are reported in Supplementary method A.2.

2.7. Electrophysiology: slice preparation and extracellular recordings

Sagittal hippocampal slices (350 µm) were carried out from additional EAE and CFA-mice at 18–22 d.p.i. Mice were deeply anesthetized with isoflurane and then decapitated. Brains were rapidly removed and chilled in an ice-cold carbogenated (*i.e.* bubbled with 95% O_2 and 5% CO_2) cutting solution containing (in mM): 120 Choline-Cl, 1.25 NaH_2PO_4, 17 glucose, 3 KCl, 1.3 $MgCl_2$ and 26 $NaHCO_3$. Sagittal slices were cut from a block of tissue using a vibratome (Microm HM650V) and then incubated in artificial cerebrospinal fluid (aCSF) 20 min at 32 °C and then 1 h at room temperature. Artificial CSF was saturated with 95% O_2 and 5% CO_2 and contained (in mM): 125 NaCl, 1.25 NaH_2PO_4, 5 glucose, 2.5 KCl, 2 $CaCl_2$, 1.3 $MgCl_2$, and 26 $NaHCO_3$.

Slices were individually transferred to a submerged recording chamber and continuously perfused (2.5–3.5 mL/min) with carbogenated and warm (30–32 °C) aCSF containing 100 µM picrotoxin (Tocris). Field excitatory post-synaptic potentials (fEPSPs) were recorded using a glass pipette (2.5–4.9 MΩ) filled with aCSF and placed in the molecular layer of the dentate gyrus or in the stratum radiatum of the CA1 region. The medial perforant pathway (MPP) in the dentate gyrus or the Schaffer collaterals in the CA1 region were stimulated using a glass electrode placed at 200 µm away from the recording pipette (Fig. 4A and D). MPP stimulation was corroborated by observing paired-pulse depression at 50 ms interpulse intervals. Basal glutamatergic synaptic transmission, evoked at 0.033 Hz, was examined by generating input/output relationships. For long-term potentiation (LTP) experiments, the stimulation intensity was set to the one producing 35–40% of maximum

Please cite this article in press as: Planche, V., et al. Selective dentate gyrus disruption causes memory impairment at the early stage of experimental multiple sclerosis. Brain Behav. Immun. (2016), http://dx.doi.org/10.1016/j.bbi.2016.11.010

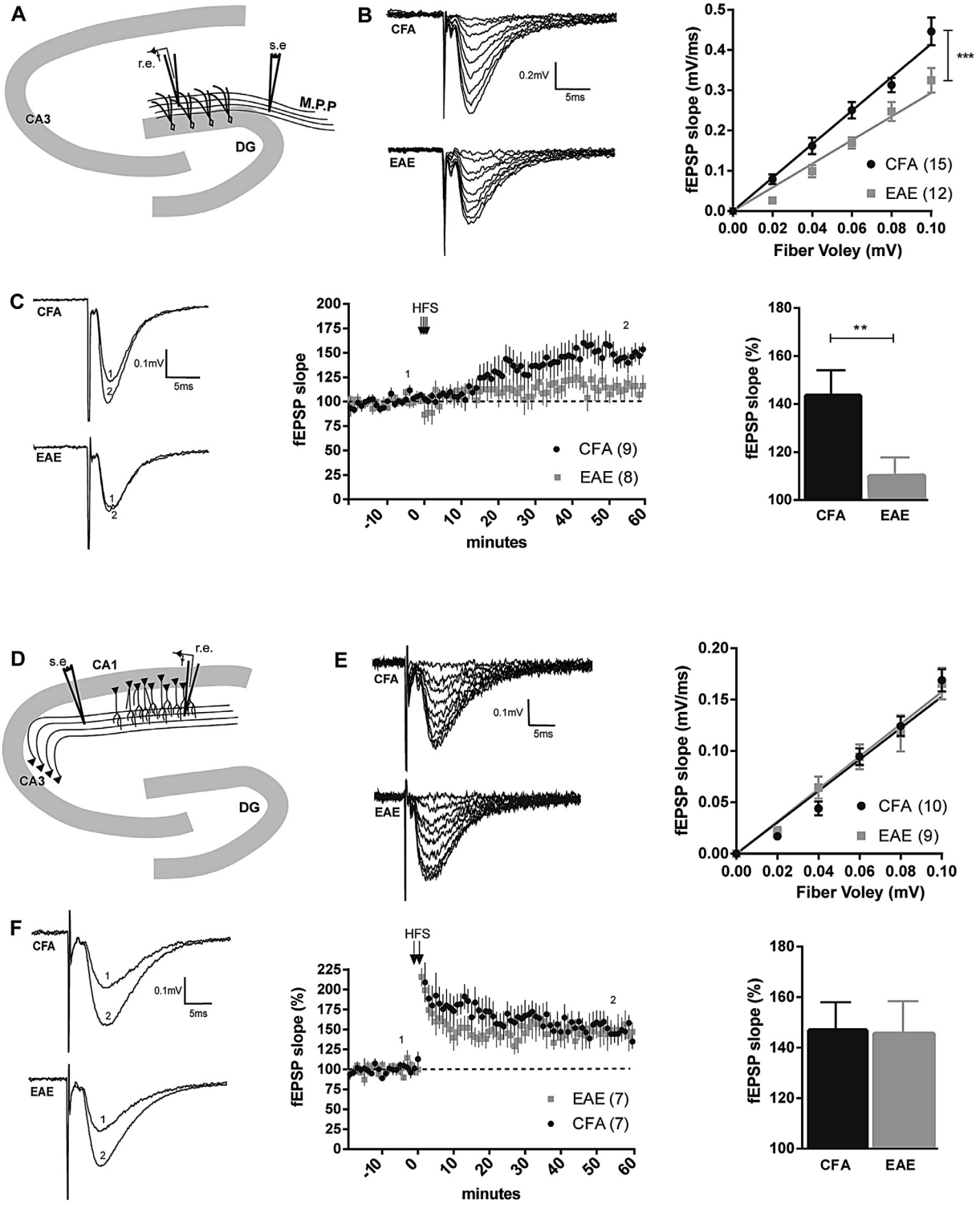

Fig. 4. Excitatory synaptic transmission and long term potentiation are decreased in the dentate gyrus but not in the CA1 area. (A and D) Schematic representation of hippocampal circuits and position of the recording and stimulating electrodes (respectively r.e. and s.e.) at the medial performant pathway (MPP) – dentate gyrus (DG) synapses (A) and the CA3-CA1 synapses (D). (B and E) (*Left*) Representative traces illustrating field excitatory post-synaptic potentials (fEPSPs) obtained in response to increasing stimulus intensity at the MPP-DG synapses (B) and at the CA3-CA1 synapses (E) and (*Right*) input/output relationship for EAE and CFA-mice at the MPP-DG synapses (EAE, n = 15 and CFA, n = 12 slices, $^{***}p < 0.001$, two-way ANOVA, (B)) and at the CA3-CA1 synapses (EAE, n = 10 and CFA, n = 9, (E)). (C and F) (*Left*) Representative traces before and after LTP induction at the MPP-DG synapses (C) and at the CA3-CA1 synapses (F) (1: last 10 min of the baseline and 2: 60 min after HFS), (*Middle*) summary plot of the average time course of fEPSP slope (% of baseline) in response to HFS and (*Right*) histogram summarizing LTP amplitude at 60 min after HFS compared to the last 10 min of the baseline in EAE and CFA-mice at the MPP-DG synapses (EAE, n = 9 and CFA, n = 8 slices, $^{**}p < 0.01$, Mann-Whitney test, (C)) and at the CA3-CA1 synapses (EAE, n = 7 and CFA, n = 7, (F)).

Please cite this article in press as: Planche, V., et al. Selective dentate gyrus disruption causes memory impairment at the early stage of experimental multiple sclerosis. Brain Behav. Immun. (2016), http://dx.doi.org/10.1016/j.bbi.2016.11.010

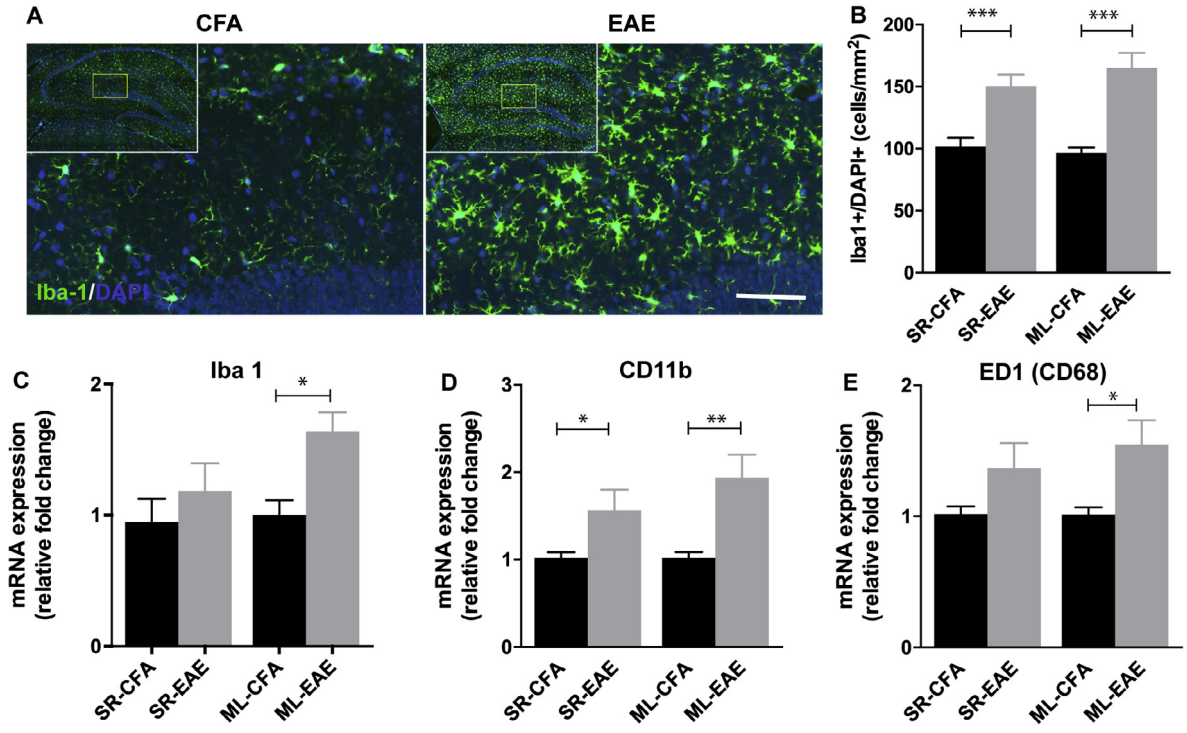

Fig. 5. Microglial activation in the dentate gyrus of EAE- mice. (A) Immunofluorescence (Iba-1 staining) and confocal imaging of microglia in the hippocampus of EAE and CFA-mice. (B) Quantification of microglial cells number in the stratum radiatum (SR) of CA1 and in the molecular layer (ML) of the dentate gyrus of EAE and CFA-mice. (C–E) Relative expression of microglia-related genes in the stratum radiatum and the molecular layer of EAE and CFA-mice. While there was a diffuse microglial proliferation in the hippocampus of EAE-mice, we can notice a differential modification of microglial transcriptional profile in the molecular layer of the dentate gyrus of EAE-mice. $^{***}p < 0.001$, *t*-test, n = 12 animals per group for histological analyses. $^{*}p < 0,05$ and $^{**}p < 0,01$, *t*-test, n = 4 (Iba1) to n = 10 (CD11b and CD68) animals per group for qPCR analyses. Scale bar: 100 μm.

fEPSP slopes. Then, LTP was induced by applying a high frequency stimulation (HFS) protocol consisting of: 100 Hz trains of stimuli for 1 s repeated at 20 s interval 2 times at CA3-CA1 synapses and 4 times at MPP-DG synapses. After HFS, fEPSPs were recorded during additional 60 min. fEPSP slopes were measured and normalized to the mean of the last 10 min of the baseline. Recordings were obtained using an Axon Multiclamp 700B amplifier (Molecular Devices). Signals were filtered at 2 kHz, digitized at 20 kHz, and analyzed using Axon Clampfit software (Molecular Devices).

2.8. Systemic injection of minocycline

Minocycline hydrochloride (Sigma) was used as a potent microglial inhibitor (Tikka et al., 2001). Minocycline was dissolved few minutes before injections in sterile isotonic PBS and administrated every 24 h by intra-peritoneal (IP) injections at a dosage of 50 mg/kg. EAE mice (EAE-MINO, n = 15) were treated from 7 d.p.i (the beginning of the motor symptoms) to 20 d.p.i. A placebo group (EAE-PBS, n = 15) received daily IP injections of PBS. The EAE score was evaluated daily by investigators blinded of the experimental conditions.

2.9. Surgical procedures and intra-hippocampal infusions of minocycline

To determine if the selective inhibition of microglial activation in the dentate gyrus was sufficient to prevent memory impairment in EAE-mice, we performed chronic local infusions of minocycline in different hippocampal subfields. Surgery and intra-hippocampal infusions were performed as described previously (Kaouane et al., 2012). Briefly, mice were anesthetized with isoflurane (2%) and secured in a Kopf stereotactic apparatus. For every mouse, stainless-steel guide cannulae (26 gauge, 8 mm length) were implanted bilaterally above the dorsal hippocampus (antero-posterior: −2 mm, mediolateral: +1.3 mm, dorsoventral: 0.8 mm; relative to dura and bregma) and then fixed to the skull with dental cement. Mice were then allowed to recover 2–3 days in their home cage before EAE induction (*i.e.* 3 weeks before behavioral experiments).

EAE-mice received every day intra-dentate gyrus or intra-CA1 bilateral infusions of minocycline (500 μg/mL, diluted in sterile PBS) or PBS alone from 7 d.p.i to 20 d.p.i. (EAE-MINO-DG, n = 17; EAE-MINO-CA1, n = 15 and EAE-MINO-PBS, n = 14; Fig. 7A and B). For infusions, the stylets normally obtruding the guide cannulae were removed. Stainless-steel cannulae (32 gauge) attached to 1 μL Hamilton syringes with catheter tubing were inserted through the guide cannulae. Cannulae had different lengths regarding the targeted subfield and infusions were performed 1.8 mm under the dura for CA1 and 2.6 mm for dentate gyrus. The syringes were fixed in a constant rate infusion pump. After preliminary experiments using Pontamine blue dye (Fig. 7A and B), we determined that a volume of 0.2 μL (per side) injected at 0.1 μL/min was optimum to allow a specific and local diffusion of drug within dorsal CA1 or dentate gyrus (Fig. 7A and B). The cannulae were left in place for an additional 90 s before removal to allow diffusion of the drug away from the tips.

2.10. Statistical analyses

Data are presented as the mean ± SEM. The Gaussian distribution was tested with Shapiro-Wilk normality test. Clinical scores and input/output curves were analyzed with two-way ANOVA. Behavioral, MRI, histological and electrophysiological quantitative data were compared between groups using ANOVA when more

Please cite this article in press as: Planche, V., et al. Selective dentate gyrus disruption causes memory impairment at the early stage of experimental multiple sclerosis. Brain Behav. Immun. (2016), http://dx.doi.org/10.1016/j.bbi.2016.11.010

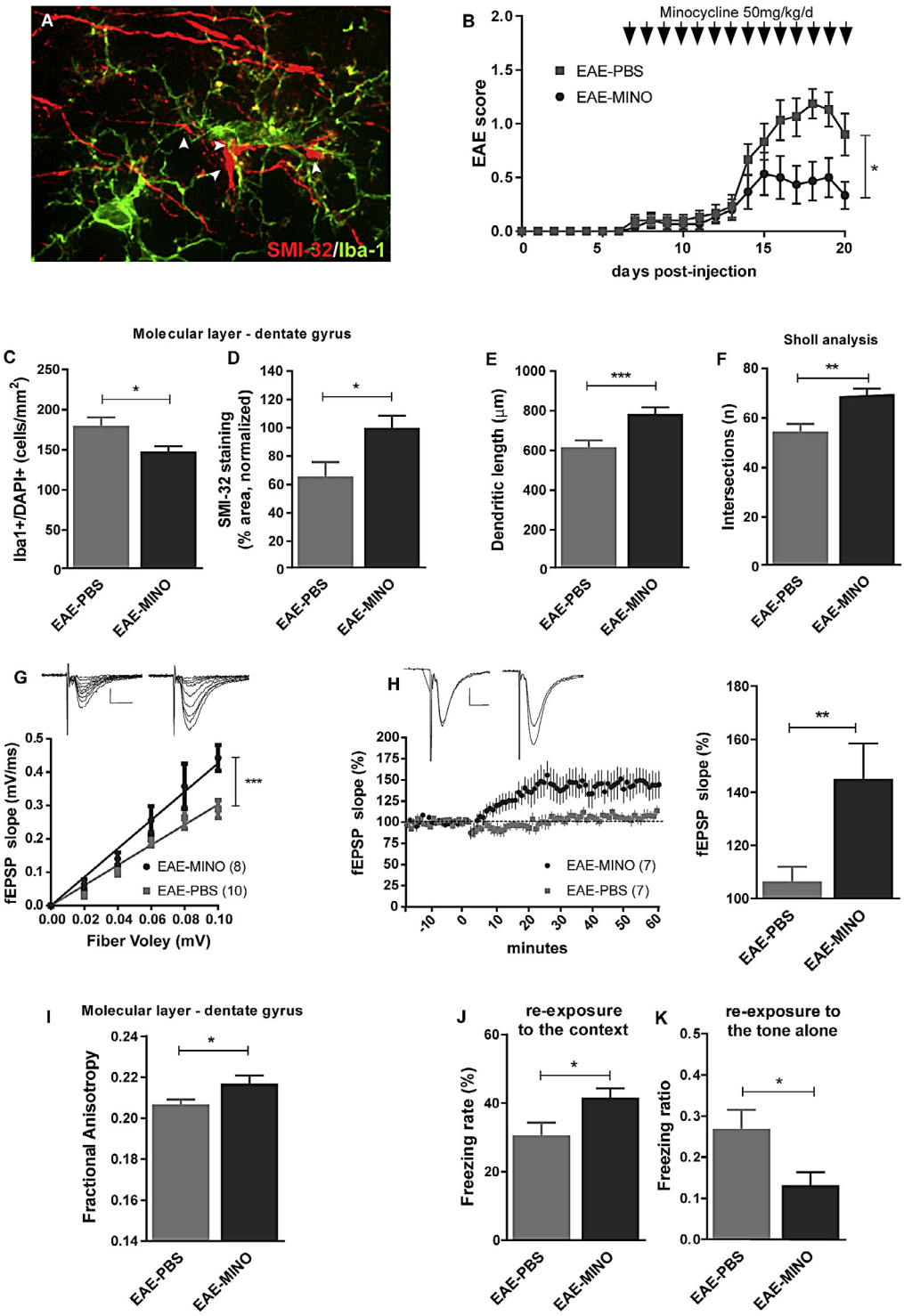

Fig. 6. The inhibition of microglial activation with minocycline treatment prevented dentate gyrus neurodegeneration, DTI changes and memory impairment in EAE-mice. (A) Z-stack projection of confocal images from the molecular layer of an EAE-PBS mouse showing activated microglial cells (Iba1, large cell body and thick arms) in contact with swelling and degenerative dendrites (SMI-32, arrowheads). (B) EAE-mice received daily injections of minocycline (50 mg/kg, n = 15) or placebo (PBS, n = 15) from 7 d.p.i. to sacrifice (vertical arrows). Treatment with minocycline decreased the clinical severity of EAE regarding the motor EAE-score ($^{*}p < 0.05$, two-way ANOVA). (C and D) Histological analyses showed that there were less microglial cells but more dendrites in the molecular layer of minocycline-treated EAE-mice (EAE-MINO) compared to placebo-treated animals (EAE-PBS) (n = 15 per group, $^{*}p < 0.05$, *t*-test). (E and F) Neurolucida neuron tracing analyses confirmed that the dendritic arbor of EAE-MINO mice were preserved compared to EAE-PBS mice (n = 30 neurons per condition, from 15 animals, $^{*}p < 0.01$, $^{***}p < 0.001$, *t*-test). (G) (Upper) Representative traces illustrating field excitatory post-synaptic potentials (fEPSPs) obtained in response to increasing stimulus intensity at the MPP-DG synapses and (Lower) input/output relationship for EAE-MINO and EAE-PBS (n = 8 and n = 10 slices respectively, $^{***}p < 0.001$, two-way ANOVA). (H) (Left) Representative traces before and after LTP induction at the MPP-DG synapses and summary plot of the average time course of fEPSP slope (% of baseline) in response to HFS in EAE-MINO and EAE-PBS mice and (Right) histogram summarizing LTP amplitude at 60 min after HFS compared to the last 10 min of the baseline and showing that LTP was preserved in EAE-MINO compared to EAE-PBS mice at the MPP-DG synapses (n = 7 slices per group, $^{**}p < 0.01$, Mann-Whitney test). (I) Fractional anisotropy in the molecular layer of the dentate gyrus was higher in EAE-MINO mice than in EAE-PBS mice (n = 15 per group, $^{*}p < 0.05$, *t*-test). (J and K) Compared to EAE-PBS mice, EAE-MINO mice displayed normal fear memory with enhanced conditioned freezing to the correct predictor of the threat, the conditioning context (J), and reduced conditioned freezing to the non-predictive tone in a familiar and safe box (K) (n = 15 per group, $^{*}p < 0.05$, *t*-test).

Please cite this article in press as: Planche, V., et al. Selective dentate gyrus disruption causes memory impairment at the early stage of experimental multiple sclerosis. Brain Behav. Immun. (2016), http://dx.doi.org/10.1016/j.bbi.2016.11.010

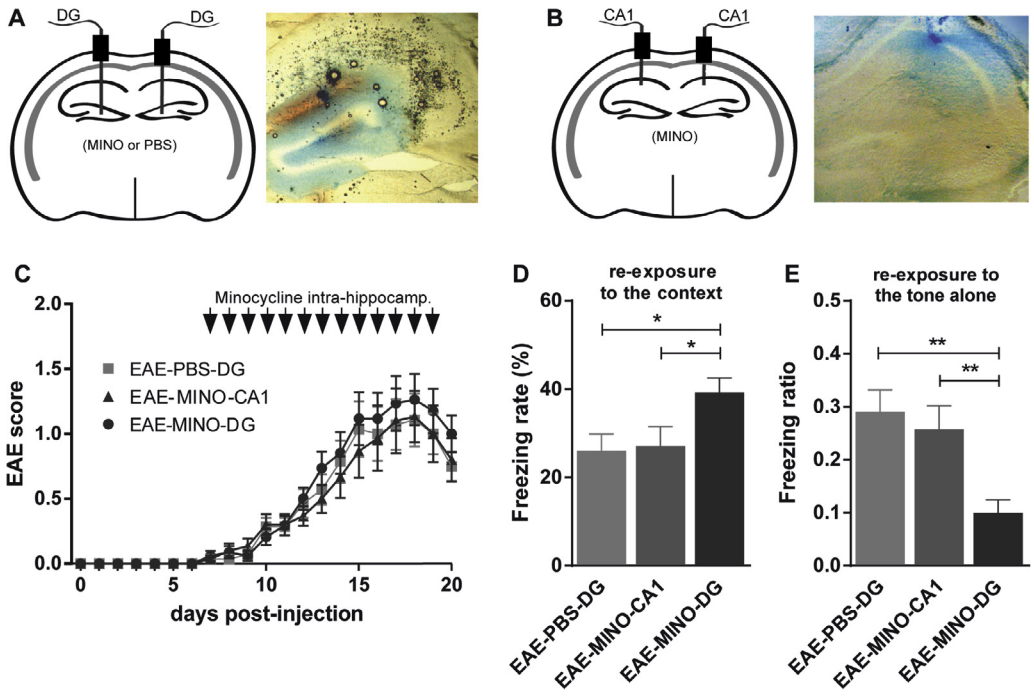

Fig. 7. Selective intra-dentate gyrus infusion of minocycline was sufficient to prevent memory impairment in EAE-mice. (A and B) EAE-mice received bilateral intra-dentate gyrus infusions of minocycline (EAE-MINO-DG, n = 17) or bilateral intra-dentate gyrus infusions of PBS (EAE-MINO-PBS, n = 14) or bilateral intra-CA1 infusions of minocycline (EAE-MINO-CA1, n = 15). In preliminary experiments, Pontamine blue dye was injected to determine optimal volume and flow rate for a local and selective diffusion into the targeted hippocampal subfields. (C) Mice were injected daily through the guide cannulae from 7 d.p.i to the day of conditioning. There was no difference between groups in disease severity according to EAE-score. (D and E) Compared to EAE-MINO-CA1 mice and EAE-PBS-DG mice, EAE-MINO-DG mice displayed normal fear memory with preserved conditioned freezing to the conditioning context (D), and reduced conditioned freezing to the non-predictive tone in a familiar and safe box (E). ($^{*}p < 0.05$, $^{**}p < 0.01$, Tukey's multiple comparisons test after ANOVA).

than two groups were compared (and Tukey's multiple comparisons test for *post hoc* multiple comparisons) or unpaired *t*-tests (or Mann-Whitney tests) when two groups were compared (except for quantification of Caspase-3 staining where a Fisher's exact test was used). In order to perform MRI-histological correlation, we used Pearson's correlations for univariate analyses and then multiple linear regressions to model the relationship between MRI data (dependent variables) and histological data (independent variables). Statistical analyses were performed with Prism 6.0 (GraphPad). A p-value <0.05 was deemed significant.

3. Results

3.1. EAE-mice presented an early hippocampal-dependent memory deficit

Twenty days post-immunization (d.p.i), EAE-mice were experiencing first clinical expression of motor symptoms but were all still ambulatory with a mean clinical score of 1.6 ± 0.20 (Fig. 1A). To assess hippocampal long-term memory we used a dedicated contextual fear conditioning procedure (Fig. 1B). EAE-mice displayed significantly less conditioned freezing than control CFA-mice, when they were re-exposed to the predictive context (freezing rate: 23.3% vs 42.1%, p = 0.011, Figs. 1C and A.1A). This suggests that the functional integrity of the hippocampus was impaired because mice showed a deficit in the identification of the environment in which they previously received footshocks as predictor of the threat. Moreover, the same EAE-mice displayed significantly more freezing than CFA-mice when they were re-exposed to the tone alone (which was not the relevant predictor of the threat), in a safe and familiar environment (freezing ratio: 0.380 vs 0.208, p = 0.028, Figs. 1D and A.1B). This paradoxical fear response to the tone first demonstrates that EAE-mice can freeze and even display higher conditioned fear than CFA-mice to some irrelevant cues, excluding potential bias linked to sensory or motor symptoms that would have hindered EAE-mice to feel shock or to display freezing. Second, this maladaptive fear response to the tone attests of an altered hippocampal-amygdala interaction to the detriment of the hippocampal function in EAE-mice. Indeed, such amygdala-dependent elemental conditioning to the most salient and simple cue (the tone) has been previously repeatedly shown when the hippocampal-dependent processing of more complex contextual information was impaired (Calandreau et al., 2006; Desmedt et al., 1999; Kaouane et al., 2012).

To definitely validate that the inability of EAE-mice to identify the complex predicting context was due to a proper hippocampal-dependent memory deficit and not to slowing of information processing speed, two other groups of EAE and CFA-mice were tested after an extended (+40%) conditioning period. As in the first experiment, EAE-mice displayed less conditioned freezing to the predictive conditioning context than CFA-mice (freezing rate: 27.2% vs 40.1%, p = 0.012, Fig. 1E). EAE-mice also showed the same paradoxical fear response to the tone, even though the freezing ratio was less pronounced than with the shorter time exposure to the conditioning context (freezing ratio: 0.189 vs −0.033, p < 0.001, Fig. 1F). This lower freezing ratio in both groups can be explained by the higher temporal distance between the tone and the shock in the extended fear conditioning paradigm, which might facilitate the processing of the tone as a non-predictive cue.

Taken together, these behavioral data indicate that a hippocampal-dependent memory deficit occurs early in the course of EAE.

Please cite this article in press as: Planche, V., et al. Selective dentate gyrus disruption causes memory impairment at the early stage of experimental multiple sclerosis. Brain Behav. Immun. (2016), http://dx.doi.org/10.1016/j.bbi.2016.11.010

3.2. Hippocampal structural changes in EAE-mice

Because we wanted to assess early cellular alteration occurring prior to irreversible atrophy, we first confirmed using *in vivo* MRI that the hippocampal volumes were not changed at this early time point. From T2-weighted images (Fig. A.2A), hippocampal volumetry (Fig. A.2B) showed no difference between EAE and CFA-mice at 20 d.p.i. (20.58 mm^3 vs 20.67 mm^3, p = 0.90, Fig. A.2C).

To screen for early regional vulnerability in the hippocampus of EAE-mice, we then used a cutting-edge high-resolution *in vivo* DTI sequence that we have optimized to allow quantifying the microscopic displacement of water within the three main hippocampal layers (Fig. 2A). Because water diffuses preferentially along the long axis of the fibers, the CA1 stratum-radiatum, the stratum-lacunosum moleculare and the molecular layer of the dentate gyrus whose fibers are perpendicularly oriented were well identified on the color-coded orientation map of the tensor (Fig. 2B and C). Quantitative measurement showed that fractional anisotropy (FA), was specifically decreased in the molecular layer of the dentate gyrus in EAE compared to CFA-mice (0.211 vs 0.225, p = 0.0093, Fig. 2D) while FA was not significantly modified in the other layers (Fig. 2D). Such decrease of FA in the molecular layer of EAE mice was driven by a decrease of axial diffusivity (AD) (0.561 vs 0.580 μm^2/ms, p = 0.030, Fig. 2E), while radial diffusivity (Fig. 2F) and mean diffusivity were not significantly changed (respectively 0.404 vs 0.407 μm^2/ms, p = 0.51 and 0.456 vs 0.465 μm^2/ms, p = 0.18). Finally, diffusivity parameters were not modified within the fimbria, which is the main myelinated output of the hippocampus. Taken together, these MRI experiments showed that prior to hippocampal atrophy, there was a selective decrease of the FA and AD in the molecular layer of the dentate gyrus.

3.3. Selective neurodegenerative process in the dentate gyrus of EAE-mice

Because a significant decrease of axial diffusivity is usually associated with neuritic damage (Sun et al., 2007), we first looked for potential early neuronal loss in the dentate gyrus of EAE-mice. Analysis of the dendritic marker SMI-32 revealed a dramatic decrease of the staining in the molecular layer of the dentate gyrus in EAE compared to CFA-mice (42% decrease in immunostained surface area, p = 0.0076, Fig. 3A and B). Interestingly the dendrites of the pyramidal neurons in the stratum radiatum were relatively preserved (the stratum-lacunosum moleculare contains thin axons from the perforant path and was not stained by SMI-32). In the molecular layer of the dentate gyrus, SMI-32 staining was correlated with both fractional anisotropy (r = 0.56, p = 0.0051, Fig. 3C) and axial diffusivity (r = 0.47, p = 0.024).

To better characterize this first evidence of selective vulnerability of the dentate gyrus, we performed neuromorphometric analyses of the granular neurons of the dentate gyrus, whose dendrites project in the molecular layer, and of CA1 pyramidal neurons, whose dendrites project in the stratum radiatum. Under our sampling conditions, there was no significant morphological difference between EAE and CFA-mice regarding the dendrites of CA1 pyramidal neurons in the stratum radiatum (Figs. 3D, E, F and A.3A, B). However, the total dendritic length and the complexity of the dendritic arbor were decreased in the granular neurons of EAE-mice compared to CFA-animals (respectively 517 μm vs 679 μm, p = 0.014 and 46.4 vs 58.5 intersections, p = 0.039, Figs. 3D, E, F and A.3C, D). These data demonstrate a selective neuritic degeneration in the dentate gyrus. Thus, we decided to look at neuronal apoptosis in the granular cell layer of the dentate gyrus and the pyramidal cell layer of CA1 using activated Caspase-3 staining (Fig. 3G). The occurrence of Caspase-3 positive neurons in the dentate gyrus was significantly higher in slices obtained from EAE-mice compared to CFA-animals (8 neurons of 36 slices vs 1 neuron of 36 slices, p = 0.028, Fig. 3H). Such increase in Caspase-3 positive neurons in the dentate gyrus was not observed in the pyramidal cell layer of EAE-mice. These results further strengthen the hypothesis of a selective neurodegenerative process that takes place at an early stage of the disease in the dentate gyrus and that is characterized by both dendritic loss and neuronal death (even though an alternative explanation could be an impaired phagocytosis of apoptotic cells rather than a decreased survival (Abiega et al., 2016)).

Because one specific property of the dentate gyrus is its ability to produce newborn neurons throughout adulthood, we also analyzed doublecortin (DCX) immature neurons (less than 4 weeks old neuroblasts) in the sub-granular zone of EAE and CFA-mice (Fig. 3I). There was no significant difference between the two groups after DCX/DAPI cells counting (Fig. 3J) probably because at this early time point (Giannakopoulou et al., 2013) inflammation enhances the division of radial-glia cells more than the division leading to newborn neurons.

Taken together, histological analyses are thus in agreement with our DTI results, thereby confirming the selective vulnerability of the dentate gyrus at this early stage of EAE.

3.4. Impaired excitatory synaptic transmission in the dentate gyrus of EAE-mice

To investigate functional consequences of this neurodegenerative process specifically in the dentate gyrus at this early stage of EAE, we analyzed excitatory glutamatergic synaptic transmission at two different synapses in acute hippocampal slice preparations. We first investigated excitatory synaptic transmission at synapses formed by the medial perforant path (MPP, axons coming from the enthorinal cortex) and the dendrites of dentate granule cells in the molecular layer of the dentate gyrus (Fig. 4A). To this end, fEPSPs were evoked at different stimulation intensities to assess the input/output (I/O) relationship at these synapses. Interestingly, fEPSPs slope were significantly lower in EAE-mice in comparison to CFA-mice (F = 17.18, p = 0.0006, Fig. 4B). We then investigated the I/O relationship at CA3-CA1 excitatory synapses and no impairment was detected in EAE mice (Fig. 4D and E). These results confirm the selective vulnerability of the dentate gyrus to early pathophysiological processes in EAE. Indeed, the decreased basal synaptic excitatory transmission recorded at the MPP-DG synapses probably results from synaptic loss that is likely to be associated with the dendritic loss observed with DTI and histological methods.

3.5. Decreased synaptic plasticity in the dentate gyrus of EAE-mice

We then tested whether LTP of hippocampal excitatory synaptic transmission, a process known as the cellular substrate of episodic memory (Bliss and Lomo, 1973), was affected in EAE-mice and whether it could be synapse specific. LTP was elicited with a high-frequency stimulation (HFS) protocol of the MPP or the Schaffer collateral pathway and recorded in the molecular layer of the dentate gyrus or in CA1 stratum radiatum respectively. Importantly, there was a strong decrease in the level of LTP at the MPP-DG synapses in EAE compared to CFA-mice (110.2% vs 143.5%, p = 0.001, Fig. 4C) whereas LTP was not impaired at the CA3-CA1 synapses (146.8% in EAE-mice vs 145.5% in CFA-mice, p = 0.87, Fig. 4F). These results indicate that in the dentate gyrus of EAE-mice, on top of synaptic loss, the remaining synapses exhibit impaired plasticity properties.

Please cite this article in press as: Planche, V., et al. Selective dentate gyrus disruption causes memory impairment at the early stage of experimental multiple sclerosis. Brain Behav. Immun. (2016), http://dx.doi.org/10.1016/j.bbi.2016.11.010

3.6. Differential microglial activation in the dentate gyrus of EAE-mice

Because EAE potentially impacts all glial cells during the course of the disease and because all glial cell dysfunctions potentially impact neuronal function and survival (Brosnan and Raine, 2013), we investigated possible myelin, astrocytic and microglial alterations in the hippocampus of EAE-mice. Myelin staining with MBP did not show any demyelinating area in the hippocampus, even after quantitative analysis (Fig. A.4A and C). There was also neither obvious difference in astrocyte morphology after the analysis of GFAP staining area nor increase of astrocyte number after GFAP/DAPI cell counting (Fig. A.4B and D) in none of the hippocampal layers. ED1(CD68) and CD3 staining revealed the absence of macrophages and T lymphocytes infiltration in the hippocampus of EAE-mice whereas these markers were detected in typical demyelinating lesions in the spinal cord (Fig. A.5), as classically reported at this stage of the disease ('t Hart et al., 2011).

Microglial cells exhibited morphological changes including larger cell bodies, thicker processes (Fig. 5A) and higher percentage of staining area after quantitative analyses in both the stratum radiatum (respectively 7.24% for EAE-mice vs 3.95% for CFA-mice, $p = 0.011$) and in the molecular layer of the dentate gyrus (7.25% vs 3.57%, $p = 0.007$). We also found an increase in microglial cells number in EAE-mice (50–70% increase after Iba-1/DAPI cell counting) in both the stratum radiatum (150.4 vs 101.6 cells/mm^2, $p = 0.0004$) and the molecular layer of the dentate gyrus (165.3 vs 96.6 cells/mm^2, $p < 0.0001$) (Fig. 5B). As morphological analyses show diffuse increase in microglial cells number in the whole hippocampus (although slightly higher in the dentate gyrus), we decided to look at mRNA expression profile in hippocampal subregions. Interestingly, mRNA expression level of microglial markers such as Iba-1 and ED1(CD68) was significantly increased in the molecular layer of the dentate gyrus of EAE-mice (1.64 in ML-EAE vs 1.00 in ML-CFA for Iba1, $p = 0.013$ and 1.55 in ML-EAE vs 1.01 in ML-CFA for ED1(CD68), $p = 0.012$, Fig. 5C and E) but not significantly in CA1. The expression level of CD11b in EAE-mice compared to CFA-mice was enhanced in both the molecular layer of the dentate gyrus and the stratum radiatum of CA1 (1.94 in ML-EAE vs 1.02 in ML-CFA $p = 0.0030$ and 1.56 in SR-EAE vs 1.02 in SR-CFA, $p = 0.038$, Fig. 5D).

To test whether such microglial activation is one of the biological substrates of DTI abnormalities observed in the hippocampus of EAE-mice (Fig. 2), we further looked for MRI-histological correlations. None of these glial alterations were sufficient by themselves to contribute independently to the signal measured *in vivo* with DTI. After a backward stepwise selection of all the histological metrics, the final model of MR-to-histology correlation amounted to a univariate relationship between FA/AD and dendritic loss ($r^2 = 0.32$, $p = 0.0051$ and $r^2 = 0.22$, $p = 0.024$ respectively, Table A.1).

3.7. Systemic inhibition of microglial activation prevented anatomical, electrophysiological and behavioral abnormalities

The transcriptional profile of microglial markers in the molecular layer of the dentate gyrus, together with the selective neurodegeneration observed in this hippocampal subfield suggest a link between this 2 processes. Furthermore, the co-staining of Iba-1 and SMI-32 in the molecular layer of the dentate gyrus of EAE-mice revealed that microglia extended processes around dendrites and that microglial cell bodies were appended on swelling neurites, suggesting that these cells could induce the neurodegeneration described above (Fig. 6A). To test this hypothesis, we used minocycline, a well-known inhibitor of microglial activation (Kobayashi et al., 2013). Two groups of EAE-mice were treated daily with minocycline (EAE-MINO, 50 mg/kg) or saline injection (EAE-PBS) after the onset of the motor symptoms (7 d.p.i).

Minocycline treatment significantly reduced motor symptoms in EAE-mice with an early stabilization of the neurological deficit ($F = 5.27$, $p = 0.029$, Fig. 6B), as previously described (Popovic et al., 2002). As expected, on histological analyses, microglial cells number was lower in EAE-MINO compared to EAE-PBS mice (147.8 vs 179.7 cells/mm^2, $p = 0.019$, Figs. 6C and A.6A, B). As a consequence, neurofilament staining was preserved in the molecular layer of EAE-MINO mice compared to EAE-PBS (35% increase, $p = 0.017$, Figs. 6D and A.6C, D). Neuron tracing analyses (Fig. A.6E and F) confirmed that dendritic length was higher in EAE-MINO mice than in EAE-PBS mice (784.8 μm vs 616.5 μm, $p = 0.0009$, Fig. 6E) and that dendritic arbor complexity was also higher in EAE-MINO mice (68.8 vs 54.4 intersections, $p = 0.0022$, Fig. 6F). Basal excitatory synaptic transmission was preserved at the MPP-DG synapses in EAE-MINO mice as revealed by measuring I/O relationships ($F = 18.81$, $p < 0.0001$, Fig. 6G). The treatment also prevented LTP impairment in the DG (145.1% in EAE-MINO mice vs 106.3% on EAE-PBS mice, $p = 0.01$, Fig. 6H). Such protective effect was measurable *in vivo* on MRI metrics as FA was higher in EAE-MINO mice compared to EAE-PBS mice (0.217 vs 0.207, $p = 0.045$, Fig. 6I). Finally, in the contextual conditioning procedure EAE-MINO mice showed a higher conditioned fear to the predictive conditioning context compared to EAE-PBS mice (freezing rate: 41.6% vs 30.6%, $p = 0.021$, Fig. 6J) and a lower conditioned fear to the non-predictive tone (freezing ratio: 0.131 vs 0.269, $p = 0.021$, Fig. 6K), demonstrating that minocycline treatment prevented the early memory impairment observed in EAE-mice.

3.8. Selective inhibition of dentate gyrus microglial activation was sufficient to prevent memory impairment in EAE-mice

Because we could not exclude that the protection against memory impairment after systemic injections of minocycline could involve additional mechanisms on top of dentate gyrus protection, we selectively infused minocycline in the dentate gyrus of EAE-mice (EAE-MINO-DG) daily from 7 to 20 d.p.i. Intra-dentate gyrus infusions of PBS (EAE-PBS-DG) and intra-CA1 infusions of minocycline (EAE-MINO-CA1) served as controls. Preliminary experiments with blue-dye infusions were used to define the appropriate volume and flow rate to restrict diffusion of drugs to the region of interest (Fig. 7A and B). As expected from intra-hippocampal injections, there was no difference between minocycline and PBS infusions regarding the EAE-scores (which essentially reflect motor symptoms, Fig. 7C). In the contextual fear conditioning procedure, only the EAE-MINO-DG mice were protected against memory impairment as they showed a higher conditioned fear to the predictive conditioning context compared to both EAE-MINO-CA1 mice and EAE-PBS-DG mice (freezing rate: 39.23%, 27.15% and 26.04% respectively, $F = 3.88$, $p = 0.028$, Fig. 7D) and a lower conditioned fear to the non-predictive tone (freezing ratio: 0.099, 0.258 and 0.290 respectively, $F = 8.09$, $p = 0.001$, Fig. 7E). There was no significant behavioral difference between EAE-MINO-CA1 and EAE-PBS-DG mice demonstrating that hippocampal microglial activation outside the dentate gyrus was not involved in early memory impairment in EAE-mice. Taken together, these experiments formally establish a causal link between selective dentate gyrus disruption and memory impairment.

4. Discussion

We provided results highlighting the selective vulnerability of the dentate gyrus to microglial activation at the early stage of

Please cite this article in press as: Planche, V., et al. Selective dentate gyrus disruption causes memory impairment at the early stage of experimental multiple sclerosis. Brain Behav. Immun. (2016), http://dx.doi.org/10.1016/j.bbi.2016.11.010

experimental multiple sclerosis and its involvement in early memory impairment. These data introduce the concept of differential vulnerability of the dentate gyrus in the context of multiple sclerosis; the potential of microglia blockers to maintain the cognitive performances; and the possibility to monitor such effects *in vivo* with high-resolution DTI.

In previous studies on EAE-mice, spatial memory dysfunction was investigated with the Barnes maze, the Morris water maze or object exploration/recognition. Therefore, memory impairment in EAE was reported at later stages, during the recovery of motor symptoms, after selection of animals with mild motor symptoms or during the initial immunization period before EAE onset (Ziehn et al., 2010; Rahn et al., 2012; D'Intino et al., 2005; Kim et al., 2012; Dutra et al., 2013; Di Filippo et al., 2016). Thus, a reliable and unbiased study of memory impairment, controlling for motor symptoms and slowing of information processing speed, at the early (acute) phase of EAE was still lacking. Our particular contextual conditioning paradigm allowed us to avoid and/or to control several confounding factors linked to EAE specificities such as motor or sensory deficits, amygdala lesion or disconnection. This memory task clearly shows that EAE-mice display an impaired conditioning to complex contextual cues associated with the expression of a maladaptive conditioned fear to a simple, salient, but irrelevant (non-predictive) cue. Furthermore, after local infusions, EAE-MINO-DG mice expressed a normal fear response to contextual conditioning despite sensory-motor extra-hippocampal symptoms. We can therefore conclude that the memory impairment observed in EAE-mice is due to hippocampal dysfunction specifically and not to a hippocampus-independent deficit in fear learning. It can thus be paralleled with deficits in hippocampal-dependent tasks reported in patients with early multiple sclerosis (Feuillet et al., 2007).

In diffuse brain diseases such as EAE and multiple sclerosis, it is usually difficult to understand whether a deficit is due to global brain damage or to more focal alteration and this question is impossible to solve in humans. By using local infusions of minocycline we could demonstrate here that early memory impairment in EAE is selectively due to a microglia-mediated dentate gyrus disruption. Interestingly, a similar memory impairment has been previously associated with deficits in dentate gyrus activation in a mouse model of post-traumatic stress disorder (Kaouane et al., 2012). The link between dentate gyrus dysfunction and impaired contextual learning has also been described in recent experiments using optogenetic techniques in the mouse brain (Kheirbek et al., 2013; Liu et al., 2012).

This preferential vulnerability of the dentate gyrus results in an impairment of basal synaptic transmission and synaptic plasticity in EAE-mice. Previous studies reported that LTP was preserved at CA3-CA1 synapses at the acute phase of the disease (Prochnow et al., 2013; Di Filippo et al., 2013; Novkovic et al., 2015). One of them (Novkovic et al., 2015) showed that, while preserved at the early stage, LTP became impaired in CA1 at the chronic-progressive stage of the disease (40 d.p.i). Then, we can hypothesize that the dysfunction of hippocampal neurons extends beyond the dentate gyrus during the course of EAE. Furthermore, in another study, LTP and long term depression (LTD) were reported to be preserved in CA1 area whereas LTD was disrupted in the superior colliculus and the cerebellum at the same early stage (Prochnow et al., 2013). In terms of synaptic transmission and plasticity, this suggests that some brain regions are more vulnerable than others to the inflammatory mechanisms occurring in EAE. In view of our results, we expand this concept to the hippocampal trisynaptic loop itself where synaptic transmission and plasticity are altered in the dentate gyrus but not in CA1 region. Finally, such synaptic deficits provide a strong cellular and functional explanation to the early memory impairment of EAE-mice.

In humans, the fundamental role of dentate gyrus granule cells compared to CA1 pyramidal neurons in declarative memory acquisition has been suggested (Coras et al., 2014) but could not be easily demonstrated in the context of early multiple sclerosis. Post-mortem studies have revealed that CA1 and dentate gyrus were the most affected regions in late multiple sclerosis, probably because they are encompassed by CSF, meningeal follicles and cytotoxic factors (Papadopoulos et al., 2009). Furthermore, the decrease of synaptophysin, a presynaptic protein involved in synaptic vesicle release, has been shown to be more important in demyelinated dentate gyrus than in demyelinated CA1, suggesting that dentate gyrus neurons could be more vulnerable to inflammatory mechanisms (Dutta et al., 2011). *In vivo* MRI studies of hippocampal subfields in patients with multiple sclerosis described controversial results. In one hand, some authors described that CA1 sub-region is the most atrophic field in the hippocampus of patients with multiple sclerosis (Sicotte et al., 2008; Longoni et al., 2015). In the other hand, a recent study, by using a hippocampal radial mapping analysis, described an expansion of the dentate gyrus related to memory function (Rocca et al., 2015) while another group has correlated the CA2/3-dentate gyrus volume with depressive symptoms and cortisol levels in patients with multiple sclerosis (Gold et al., 2010). However, such volumetric analyses might reflect late modifications that do not presume the early neurodegenerative mechanisms. Furthermore, MRI failed to precisely isolate and measure dentate gyrus itself (the structure being usually confounded with CA2/3 regions on morphological MRI). In this context, our results on EAE provide strong evidence of the vulnerability of the dentate gyrus and focus on its early nature, prior to demyelination, with consistent behavioral, MRI, histological and electrophysiological correlates. Furthermore, we were able to demonstrate a causal link between this vulnerability and microglial activation.

The link between microglial activation, demyelination, neurodegeneration and disability has been suggested in multiple sclerosis by post-mortem histological studies (Peterson et al., 2001), PET imaging in patients with a progressive form of the disease (Politis et al., 2012) and EAE induction in transgenic mice (Heppner et al., 2005). This association is highly complex as noxious effect of activated microglia can be balanced by beneficial role for tissue repair (Aguzzi et al., 2013). Here, we suggest a relationship between microglial activation, neurodegeneration and memory impairment, and we extend these data by identifying the particular vulnerability of the dentate gyrus to this process. Indeed, 20 d.p.i., there was neither macrophage nor lymphocytic infiltration in the hippocampus and there was also no demyelination to explain dendrite transection. Furthermore, the inhibition of microglial activation with minocycline protected mice from dendritic damages, synaptic plasticity disruption and memory impairment, demonstrating that microglial activation in EAE dentate gyrus is deleterious for the structure and the function of granular neurons. Because intra-dentate gyrus inhibition of microglial activation prevents memory impairment in EAE-mice, we can exclude that minocycline acts through indirect mechanisms, such as peripheral immune response modulation or matrix metalloproteinase inhibition (Chen et al., 2011) while direct neuroprotective effect of minocycline might still be possible (Möller et al., 2016).

Despite a diffuse increase in microglial cells number in the hippocampus of EAE-mice, we described here at the transcriptional level a differential pattern of activation within the dentate gyrus, that was absent or less pronounced in CA1. Given that there could be regional differences in microglial phenotype in the brain (Aguzzi et al., 2013), we can hypothesize that microglia is already "primed" in the dentate gyrus to control newborn neurons and circuits in physiological conditions, leading to the early aberrant

Please cite this article in press as: Planche, V., et al. Selective dentate gyrus disruption causes memory impairment at the early stage of experimental multiple sclerosis. Brain Behav. Immun. (2016), http://dx.doi.org/10.1016/j.bbi.2016.11.010

activation that we described here in case of inflammatory disease. Future studies will need to explore the profile of inflammatory markers in each layer. Future studies will also need to address the mechanistic pathways responsible for pathological microglia-neuron interactions within the dentate gyrus. Recent studies in neuroinflammation suggest that it could involve the complement pathway (Michailidou et al., 2015), the platelet-activating factor receptor (Bellizzi et al., 2016), the fractalkine receptor (Rogers et al., 2011), the interleukin-1β (Nisticò et al., 2013), the NADPH oxydase (Di Filippo et al., 2016) or indirect mechanisms through astrocytes and the multipartite synapse (Habbas et al., 2015).

This study highlights the therapeutic potential of minocycline in multiple sclerosis (Chen et al., 2011). Its positive effect on myelitis symptoms in EAE has already been described (Popovic et al., 2002) and a small phase II clinical trial in patients with multiple sclerosis demonstrated a trend toward the efficiency of minocycline on usual surrogate MRI criteria (Metz et al., 2009). Furthermore, a recent study in another EAE model of the disease, demonstrated that minocycline could prevent memory dysfunction at the chronic phase of the disease, after the recovery of motor symptoms, suggesting that our results are still relevant at later stages (Di Filippo et al., 2016). Then, in future human clinical trials, it would be of great interest to evaluate the neuroprotective effect of this drug with cognitive evaluation and advanced MRI techniques such as DTI to assess the microstructure of the hippocampus, particularly the dentate gyrus.

From the translational point of view, this study is a proof-of-concept that early neuritic damage in the dentate gyrus can be monitored *in vivo* by DTI, prior to hippocampal measures of atrophy on T2-weighted images. Indeed, we have shown: (*i*) the independent correlation between FA/AD and neurofilament staining and (*ii*) the effect of minocycline treatment on both FA and histological measures. To our knowledge, there is only one previous *in vivo* DTI study of hippocampal subfields with MRI-histological correlations, on an epileptic rat model (Laitinen et al., 2010). Interestingly, several months after status epilepticus, the authors have reported an increased FA in the dentate gyrus, explained by an increased AD and correlated with neuritic sprouting in histological analyses. It represents an external validation of our findings because opposite histological mechanisms (*i.e.* neuritic sprouting vs neuritic loss) lead to opposite DTI parameters changes (*i.e.* FA/AD increased vs FA/AD decreased). This finding opens perspectives to use high resolution hippocampal DTI as a surrogate marker for phase II clinical trial to measure the effects of treatments on memory impairment and neurodegeneration in multiple sclerosis and also to test the selective vulnerability of the dentate gyrus in patients.

To summarize, the present study indicates that early hippocampal-dependent memory impairment in experimental multiple sclerosis is caused by dentate gyrus vulnerability. We provide compelling results from several complementary techniques converging on this same finding. Accordingly, the concept of differential regional vulnerability within the hippocampal formation must be extended to multiple sclerosis as microglial activation was causing dendritic loss, neuronal death and synaptic plasticity disruption selectively in the dentate gyrus at the early stage of EAE. Furthermore, in order to facilitate future studies in humans, we have demonstrated that these cellular alterations are measurable *in vivo* with DTI and that they can be prevented by minocycline treatment.

Funding

This work was supported by Inserm, Université de Bordeaux, and by the Fondation pour la Recherche Médicale (Equipe FRM to SHO). The work was further supported by public grants from the French Agence Nationale de la Recherche within the context of the Investments for the Future program referenced ANR-10-LABX-57 named TRAIL (project IBIO-NI) and ANR-10-LABX-43 named BRAIN (Project MEMO-MS). The microscopy was done in the Bordeaux Imaging Center, a service unit of the CNRS-INSERM and Bordeaux University, member of the national infrastructure France BioImaging. The 4.7 T animal scanner was supported by the FLI (ANR-11-INBS-0006). VP received personal support from Clermont-Ferrand University Hospital and the Inserm MD-PhD program (Ecole de l'Inserm – Liliane Bettencourt).

Author contributions

Conceived and designed the experiments: VP, AP, BH, BB, VD, AD, SHO, TT. Performed the experiments: VP, BH, EGD, GR, ND, MM, TLL, TT. Analyzed the data: VP, AP, AD, TT. Wrote the manuscript: VP and TT. All the authors have revised the manuscript critically for important intellectual content.

Acknowledgments

The microscopy was done in the Bordeaux Imaging Center, a service unit of the CNRS-INSERM and Bordeaux University, member of the national infrastructure France BioImaging. The help of Christel Poujol and Sebastien Marais (Bordeaux Imaging Center) is acknowledged as well as Philippe Ciofi and Lucie Blaszczyk (INSERM U1215) for technical supports regarding histology and microscopy experiments. We thank Laurent Brayda-Bruno (INSERM U1215) for technical support with behavioral experiments and his preliminary experiments for intra-dentate gyrus infusions of drugs.

Appendix A. Supplementary data

Supplementary data associated with this article can be found, in the online version, at http://dx.doi.org/10.1016/j.bbi.2016.11.010.

References

Abiega, O., Beccari, S., Diaz-Aparicio, I., Nadjar, A., Layé, S., Leyrolle, Q., Gómez-Nicola, D., Domercq, M., Pérez-Samartín, A., Sánchez-Zafra, V., Paris, I., Valero, J., Savage, J.C., Hui, C.-W., Tremblay, M.-È., Deudero, J.J.P., Brewster, A.L., Anderson, A.E., Zaldumbide, L., Galbarriatu, L., Marinas, A., Vivanco, M.D.M., Matute, C., Maletic-Savatic, M., Encinas, J.M., Sierra, A., 2016. Neuronal hyperactivity disturbs ATP microgradients, impairs microglial motility, and reduces phagocytic receptor expression triggering apoptosis/microglial phagocytosis uncoupling. PLoS Biol. 14, e1002466.

Aguzzi, A., Barres, B.A., Bennett, M.L., 2013. Microglia: scapegoat, saboteur, or something else? Science 339, 156–161.

Bellizzi, M.J., Geathers, J.S., Allan, K.C., Gelbard, H.A., 2016. Platelet-activating factor receptors mediate excitatory postsynaptic hippocampal injury in experimental autoimmune encephalomyelitis. J. Neurosci. 36, 1336–1346.

Bliss, T.V., Lomo, T., 1973. Long-lasting potentiation of synaptic transmission in the dentate area of the anaesthetized rabbit following stimulation of the perforant path. J. Physiol. (Lond.) 232, 331–356.

Brosnan, C.F., Raine, C.S., 2013. The astrocyte in multiple sclerosis revisited. Glia 61, 453–465.

Bustin, S.A., Benes, V., Garson, J.A., Hellemans, J., Huggett, J., Kubista, M., Mueller, R., Nolan, T., Pfaffl, M.W., Shipley, G.L., Vandesompele, J., Wittwer, C.T., 2009. The MIQE guidelines: minimum information for publication of quantitative real-time PCR experiments. Clin. Chem. 55, 611–622.

Calandreau, L., Trifilieff, P., Mons, N., Costes, L., Marien, M., Marighetto, A., Micheau, J., Jaffard, R., Desmedt, A., 2006. Extracellular hippocampal acetylcholine level controls amygdala function and promotes adaptive conditioned emotional response. J. Neurosci. 26, 13556–13566.

Centonze, D., Muzio, L., Rossi, S., Cavasinni, F., De Chiara, V., Bergami, A., Musella, A., D'Amelio, M., Cavallucci, V., Martorana, A., Bergamaschi, A., Cencioni, M.T., Diamantini, A., Butti, E., Comi, G., Bernardi, G., Cecconi, F., Battistini, L., Furlan, R., Martino, G., 2009. Inflammation triggers synaptic alteration and degeneration in experimental autoimmune encephalomyelitis. J. Neurosci. 29, 3442–3452.

Chen, X., Ma, X., Jiang, Y., Pi, R., Liu, Y., Ma, L., 2011. The prospects of minocycline in multiple sclerosis. J. Neuroimmunol. 235, 1–8.

Chiaravalloti, N.D., DeLuca, J., 2008. Cognitive impairment in multiple sclerosis. Lancet Neurol. 7, 1139–1151.
Citri, A., Malenka, R.C., 2008. Synaptic plasticity: multiple forms, functions, and mechanisms. Neuropsychopharmacology 33, 18–41.
Compston, A., Coles, A., 2008. Multiple sclerosis. Lancet 372, 1502–1517.
Coras, R., Pauli, E., Li, J., Schwarz, M., Rössler, K., Buchfelder, M., Hamer, H., Stefan, H., Blumcke, I., 2014. Differential influence of hippocampal subfields to memory formation: insights from patients with temporal lobe epilepsy. Brain 137, 1945–1957.
Desmedt, A., Garcia, R., Jaffard, R., 1999. Vasopressin in the lateral septum promotes elemental conditioning to the detriment of contextual fear conditioning in mice. Eur. J. Neurosci. 11, 3913–3921.
Di Filippo, M., Chiasserini, D., Gardoni, F., Viviani, B., Tozzi, A., Giampà, C., Costa, C., Tantucci, M., Zianni, E., Boraso, M., Siliquini, S., de Iure, A., Ghiglieri, V., Colcelli, E., Baker, D., Sarchielli, P., Fusco, F.R., Di Luca, M., Calabresi, P., 2013. Effects of central and peripheral inflammation on hippocampal synaptic plasticity. Neurobiol. Dis. 52, 229–236.
Di Filippo, M., de Iure, A., Giampà, C., Chiasserini, D., Tozzi, A., Orvietani, P.L., Ghiglieri, V., Tantucci, M., Durante, V., Quiroga-Varela, A., Mancini, A., Costa, C., Sarchielli, P., Fusco, F.R., Calabresi, P., 2016. Persistent activation of microglia and NADPH drive hippocampal dysfunction in experimental multiple sclerosis. Sci. Rep. 6, 20926.
D'Intino, G., Paradisi, M., Fernandez, M., Giuliani, A., Aloe, L., Giardino, L., Calzà, L., 2005. Cognitive deficit associated with cholinergic and nerve growth factor down-regulation in experimental allergic encephalomyelitis in rats. Proc. Natl. Acad. Sci. U.S.A. 102, 3070–3075.
Dutra, R.C., Moreira, E.L.G., Alberti, T.B., Marcon, R., Prediger, R.D., Calixto, J.B., 2013. Spatial reference memory deficits precede motor dysfunction in an experimental autoimmune encephalomyelitis model: the role of kallikrein-kinin system. Brain Behav. Immun. 33, 90–101.
Dutta, R., Chang, A., Doud, M.K., Kidd, G.J., Ribaudo, M.V., Young, E.A., Fox, R.J., Staugaitis, S.M., Trapp, B.D., 2011. Demyelination causes synaptic alterations in hippocampi from multiple sclerosis patients. Ann. Neurol. 69, 445–454.
Feuillet, L., Reuter, F., Audoin, B., Malikova, I., Barrau, K., Cherif, A.A., Pelletier, J., 2007. Early cognitive impairment in patients with clinically isolated syndrome suggestive of multiple sclerosis. Mult. Scler. 13, 124–127.
Giannakopoulou, A., Grigoriadis, N., Bekiari, C., Lourbopoulos, A., Dori, I., Tsingotjidou, A.S., Michaloudi, H., Papadopoulos, G.C., 2013. Acute inflammation alters adult hippocampal neurogenesis in a multiple sclerosis mouse model. J. Neurosci. Res. 91, 890–900.
Gold, S.M., Kern, K.C., O'Connor, M.-F., Montag, M.J., Kim, A., Yoo, Y.S., Giesser, B.S., Sicotte, N.L., 2010. Smaller cornu ammonis 2–3/dentate gyrus volumes and elevated cortisol in multiple sclerosis patients with depressive symptoms. Biol. Psychiatry 68, 553–559.
Habbas, S., Santello, M., Becker, D., Stubbe, H., Zappia, G., Liaudet, N., Klaus, F.R., Kollias, G., Fontana, A., Pryce, C.R., Suter, T., Volterra, A., 2015. Neuroinflammatory TNFα impairs memory via astrocyte signaling. Cell 163, 1730–1741.
Heppner, F.L., Greter, M., Marino, D., Falsig, J., Raivich, G., Hövelmeyer, N., Waisman, A., Rülicke, T., Prinz, M., Priller, J., Becher, B., Aguzzi, A., 2005. Experimental autoimmune encephalomyelitis repressed by microglial paralysis. Nat. Med. 11, 146–152.
Kaouane, N., Porte, Y., Vallée, M., Brayda-Bruno, L., Mons, N., Calandreau, L., Marighetto, A., Piazza, P.V., Desmedt, A., 2012. Glucocorticoids can induce PTSD-like memory impairments in mice. Science 335, 1510–1513.
Kheirbek, M.A., Drew, L.J., Burghardt, N.S., Costantini, D.O., Tannenholz, L., Ahmari, S. E., Zeng, H., Fenton, A.A., Hen, R., 2013. Differential control of learning and anxiety along the dorsoventral axis of the dentate gyrus. Neuron 77, 955–968.
Kim, D.Y., Hao, J., Liu, R., Turner, G., Shi, F.-D., Rho, J.M., 2012. Inflammation-mediated memory dysfunction and effects of a ketogenic diet in a murine model of multiple sclerosis. PLoS One 7, e35476.
Kobayashi, K., Imagama, S., Ohgomori, T., Hirano, K., Uchimura, K., Sakamoto, K., Hirakawa, A., Takeuchi, H., Suzumura, A., Ishiguro, N., Kadomatsu, K., 2013. Minocycline selectively inhibits M1 polarization of microglia. Cell Death Dis. 4, e525.
Koenig, K.A., Sakaie, K.E., Lowe, M.J., Lin, J., Stone, L., Bermel, R.A., Beall, E.B., Rao, S. M., Trapp, B.D., Phillips, M.D., 2014. Hippocampal volume is related to cognitive decline and fornicial diffusion measures in multiple sclerosis. Magn. Reson. Imaging 32, 354–358.
Laitinen, T., Sierra, A., Pitkänen, A., Gröhn, O., 2010. Diffusion tensor MRI of axonal plasticity in the rat hippocampus. Neuroimage 51, 521–530.
Liu, X., Ramirez, S., Pang, P.T., Puryear, C.B., Govindarajan, A., Deisseroth, K., Tonegawa, S., 2012. Optogenetic stimulation of a hippocampal engram activates fear memory recall. Nature 484, 381–385.
Longoni, G., Rocca, M.A., Pagani, E., Riccitelli, G.C., Colombo, B., Rodegher, M., Falini, A., Comi, G., Filippi, M., 2015. Deficits in memory and visuospatial learning correlate with regional hippocampal atrophy in MS. Brain Struct. Funct. 220, 435–444.
Mandolesi, G., Gentile, A., Musella, A., Fresegna, D., De Vito, F., Bullitta, S., Sepman, H., Marfia, G.A., Centonze, D., 2015. Synaptopathy connects inflammation and neurodegeneration in multiple sclerosis. Nat. Rev. Neurol. 11, 711–724.
Metz, L.M., Li, D., Traboulsee, A., Myles, M.L., Duquette, P., Godin, J., Constantin, M., Yong, V.W., minocycline study investigators, G.A., 2009. Glatiramer acetate in combination with minocycline in patients with relapsing–remitting multiple sclerosis: results of a Canadian, multicenter, double-blind, placebo-controlled trial. Mult. Scler. 15, 1183–1194.
Michailidou, I., Willems, J.G.P., Kooi, E.-J., van Eden, C., Gold, S.M., Geurts, J.J.G., Baas, F., Huitinga, I., Ramaglia, V., 2015. Complement C1q-C3-associated synaptic changes in multiple sclerosis hippocampus. Ann. Neurol. 77, 1007–1026.
Mikuni, N., Babb, T.L., Chakravarty, D.N., Chung, C.K., 1998. Postnatal expressions of non-phosphorylated and phosphorylated neurofilament proteins in the rat hippocampus and the Timm-stained mossy fiber pathway. Brain Res. 811, 1–9.
Möller, T., Bard, F., Bhattacharya, A., Biber, K., Campbell, B., Dale, E., Eder, C., Gan, L., Garden, G.A., Hughes, Z.A., Pearse, D.D., Staal, R.G.W., Sayed, F.A., Wes, P.D., Boddeke, H.W.G.M., 2016. Critical data-based re-evaluation of minocycline as a putative specific microglia inhibitor. Glia 64, 1788–1794.
Nisticò, R., Mango, D., Mandolesi, G., Piccinin, S., Berretta, N., Pignatelli, M., Feligioni, M., Musella, A., Gentile, A., Mori, F., Bernardi, G., Nicoletti, F., Mercuri, N.B., Centonze, D., 2013. Inflammation subverts hippocampal synaptic plasticity in experimental multiple sclerosis. PLoS One 8, e54666.
Novkovic, T., Shchyglo, O., Gold, R., Manahan-Vaughan, D., 2015. Hippocampal function is compromised in an animal model of multiple sclerosis. Neuroscience 309, 100–112.
Papadopoulos, D., Dukes, S., Patel, R., Nicholas, R., Vora, A., Reynolds, R., 2009. Substantial archaeocortical atrophy and neuronal loss in multiple sclerosis. Brain Pathol. 19, 238–253.
Peterson, J.W., Bö, L., Mörk, S., Chang, A., Trapp, B.D., 2001. Transected neurites, apoptotic neurons, and reduced inflammation in cortical multiple sclerosis lesions. Ann. Neurol. 50, 389–400.
Planche, V., Gibelin, M., Cregut, D., Pereira, B., Clavelou, P., 2016. Cognitive impairment in a population-based study of patients with multiple sclerosis: differences between late relapsing-remitting, secondary progressive and primary progressive multiple sclerosis. Eur. J. Neurol. 23 (2), 282–289.
Politis, M., Giannetti, P., Su, P., Turkheimer, F., Keihaninejad, S., Wu, K., Waldman, A., Malik, O., Matthews, P.M., Reynolds, R., Nicholas, R., Piccini, P., 2012. Increased PK11195 PET binding in the cortex of patients with MS correlates with disability. Neurology 79, 523–530.
Popovic, N., Schubart, A., Goetz, B.D., Zhang, S.-C., Linington, C., Duncan, I.D., 2002. Inhibition of autoimmune encephalomyelitis by a tetracycline. Ann. Neurol. 51, 215–223.
Prochnow, N., Gold, R., Haghikia, A., 2013. An electrophysiologic approach to quantify impaired synaptic transmission and plasticity in experimental autoimmune encephalomyelitis. J. Neuroimmunol. 264, 48–53.
Rahn, K.A., Watkins, C.C., Alt, J., Rais, R., Stathis, M., Grishkan, I., Crainiceau, C.M., Pomper, M.G., Rojas, C., Pletnikov, M.V., Calabresi, P.A., Brandt, J., Barker, P.B., Slusher, B.S., Kaplin, A.I., 2012. Inhibition of glutamate carboxypeptidase II (GCPII) activity as a treatment for cognitive impairment in multiple sclerosis. Proc. Natl. Acad. Sci. U.S.A. 109, 20101–20106.
Rocca, M.A., Longoni, G., Pagani, E., Boffa, G., Colombo, B., Rodegher, M., Martino, G., Falini, A., Comi, G., Filippi, M., 2015. In vivo evidence of hippocampal dentate gyrus expansion in multiple sclerosis. Hum. Brain Mapp. 36, 4702–4713.
Rogers, J.T., Morganti, J.M., Bachstetter, A.D., Hudson, C.E., Peters, M.M., Grimmig, B. A., Weeber, E.J., Bickford, P.C., Gemma, C., 2011. CX3CR1 deficiency leads to impairment of hippocampal cognitive function and synaptic plasticity. J. Neurosci. 31, 16241–16250.
Ruet, A., Deloire, M., Hamel, D., Ouallet, J.-C., Petry, K., Brochet, B., 2013. Cognitive impairment, health-related quality of life and vocational status at early stages of multiple sclerosis: a 7-year longitudinal study. J. Neurol. 260, 776–784.
Shepherd, T.M., Ozarslan, E., King, M.A., Mareci, T.H., Blackband, S.J., 2006. Structural insights from high-resolution diffusion tensor imaging and tractography of the isolated rat hippocampus. Neuroimage 32, 1499–1509.
Sicotte, N.L., Kern, K.C., Giesser, B.S., Arshanapalli, A., Schultz, A., Montag, M., Wang, H., Bookheimer, S.Y., 2008. Regional hippocampal atrophy in multiple sclerosis. Brain 131, 1134–1141.
Small, S.A., 2014. Isolating pathogenic mechanisms embedded within the hippocampal circuit through regional vulnerability. Neuron 84, 32–39.
Small, S.A., Chawla, M.K., Buonocore, M., Rapp, P.R., Barnes, C.A., 2004. Imaging correlates of brain function in monkeys and rats isolates a hippocampal subregion differentially vulnerable to aging. Proc. Natl. Acad. Sci. U.S.A. 101, 7181–7186.
Sun, S.-W., Liang, H.-F., Schmidt, R.E., Cross, A.H., Song, S.-K., 2007. Selective vulnerability of cerebral white matter in a murine model of multiple sclerosis detected using diffusion tensor imaging. Neurobiol. Dis. 28, 30–38.
t Hart, B.A., Gran, B., Weissert, R., 2011. EAE: imperfect but useful models of multiple sclerosis. Trends Mol. Med. 17, 119–125.
Tikka, T., Fiebich, B.L., Goldsteins, G., Keinanen, R., Koistinaho, J., 2001. Minocycline, a tetracycline derivative, is neuroprotective against excitotoxicity by inhibiting activation and proliferation of microglia. J. Neurosci. 21, 2580–2588.
Ziehn, M.O., Avedisian, A.A., Tiwari-Woodruff, S., Voskuhl, R.R., 2010. Hippocampal CA1 atrophy and synaptic loss during experimental autoimmune encephalomyelitis. EAE Lab. Invest. 90, 774–786.

Please cite this article in press as: Planche, V., et al. Selective dentate gyrus disruption causes memory impairment at the early stage of experimental multiple sclerosis. Brain Behav. Immun. (2016), http://dx.doi.org/10.1016/j.bbi.2016.11.010